Radiation Physics and Chemistry 249 (2026) 114142

Contents lists available at ScienceDirect

Radiation Physics and Chemistry

journal homepage: www.elsevier.com/locate/radphyschem

Thermoluminescence properties and trap-kinetic analysis of undoped $BaZr(BO_3)_2$ for β-radiation dosimetry

M. Oglakci [a], Abeer S. Altowyan [b], T. Karaman [c], E.A. Cin [c], O.T. Ozmen [g], Jabir Hakami [d], O. Madkhali [d], M.B. Coban [e,f], U.H. Kaynar [g], N. Can [d,*]

[a] Physics Department, Cukurova University, Arts-Sciences Faculty, Adana, 01330, Türkiye
[b] Department of Physics, College of Science, Princess Nourah Bint Abdulrahman University, P.O. Box 84428, Riyadh, 11671, Saudi Arabia
[c] Bakircay University, Graduate School of Natural and Applied Sciences, Menemen, Izmir, Türkiye
[d] Jazan University, College of Science, Department of Physical Sciences, Physics Division, P.O. Box 114, Jazan, 45142, Kingdom of Saudi Arabia
[e] Balikesir University, Faculty of Arts and Sciences, Department of Physics, Balikesir, Turkiye
[f] Balikesir University, Science and Technology Application and Research Center, Balikesir, Turkiye
[g] Bakircay University, Faculty of Engineering and Architecture, Department of Fundamental Sciences, Menemen, Izmir, Türkiye

ARTICLE INFO

Keywords:
Thermoluminescence
Borate phosphor
Glow curve deconvolution (GCD)
Trap depth distribution
Charge redistribution

ABSTRACT

This study presents the first comprehensive thermoluminescence (TL) and kinetic characterization of $BaZr(BO_3)_2$ phosphor. Structural analysis confirms a trigonal R3c phase, while TL measurements reveal intrinsic trapping centers and a dominant dosimetric peak at ~226 °C under 365 nm detection. A preheating protocol of 170 °C for 13 s effectively suppresses shallow traps and isolates the main peak. The dose–response exhibits linear behaviour up to ~20 Gy, followed by a supralinear trend up to 500 Gy. The material demonstrates good reusability with variations within ~3–5% and a minimum detectable dose in the sub-hundred-mGy range. Kinetic analysis, supported by temperature-lag correction, yields activation energies of ~1.7–1.8 eV, indicating the presence of deep and stable traps. Glow curve deconvolution and T_m–T_{stop} analysis reveal a hierarchical trap structure. The fading behaviour is non-monotonic, with an initial slight increase within the first few hours followed by a gradual decay; the peak intensity decreases by approximately 20–30% over 1–7 days, while the integrated TL signal shows a slower decay and approaches a quasi-plateau over time. These results indicate that $BaZr(BO_3)_2$ is a promising candidate for radiation dosimetry applications.

1. Introduction

Rare-earth and transition-metal activated phosphors in oxide and borate hosts have attracted significant attention for radiation dosimetry, information storage, and persistent luminescence due to their chemical stability, wide band gaps, and ability to accommodate diverse charge-trapping centers (Ju et al., 2017; Guo et al., 2017; Xiong et al., 2020). Such materials have also been widely investigated within the broader framework of TL dosimeter (TLD) phosphor development, where trap depth, stability, and recombination efficiency determine practical performance (Satkar et al., 2021; Bos, 2017). In particular, borate-based phosphors combine low synthesis temperatures, structural flexibility, and good radiation hardness, making them attractive TL and persistent luminescence hosts (Altowyan et al., 2024; Liu et al., 2025). TL analysis in these materials provides direct access to trap depths, distributions, and recombination mechanisms that govern their dosimetric and afterglow performance and therefore plays a crucial role in understanding the charge-trapping processes responsible for luminescence behaviour, as widely discussed in classical TL theory and dosimetry literature (Chen and McKeever, 1997; Balci-Yegen et al., 2018; Alajlani et al., 2021).

Borate hosts containing alkaline-earth and rare-earth cations, such as $LaCa_4O(BO_3)_3$:Tb^{3+}, $YCa_4O(BO_3)_3$:Sm^{3+}, LaB_3O_6:Nd^{3+}, $Ba_2Mg(BO_3)_2$:RE^{3+} and BaB_4O_7:Ce^{3+}, have shown promising TL properties, including intense glow peaks, broad linear or quasi-linear dose-response ranges, acceptable fading, and good cycle-to-cycle reproducibility, highlighting their potential as dosimetric materials (Altowyan et al., 2024; Liu et al., 2025; Madkhali et al., 2025; Gavhane et al., 2020; Oglakci et al., 2025). These characteristics correspond to established performance criteria for TL dosimetric materials, including sensitivity, linear dose response, trapping stability, and reproducible glow-curve structure (Bos, 2017;

* Corresponding author.
E-mail addresses: asaltowyan@pnu.edu.sa (A.S. Altowyan), ncan@jazanu.edu.sa (N. Can).

https://doi.org/10.1016/j.radphyschem.2026.114142
Received 3 April 2026; Received in revised form 18 April 2026; Accepted 10 June 2026
Available online 11 June 2026

Chen and McKeever, 1997; McKeever, 1985).

Detailed kinetic studies using variable heating rate (VHR), initial rise (IR), T_m–T_{stop}, and computerized/general-order glow-curve deconvolution (GCD) methods are now widely employed to extract activation energies, frequency factors, kinetic orders, and to distinguish discrete versus distributed traps, as well as to clarify the thermal stability of trapping centers (Alajlani et al., 2021; Kaynar et al., 2023). These methods have been successfully applied to reveal complex multi-trap systems, anomalous heating-rate effects, and continuous trap distributions in several borate and related hosts (Alathlawi et al., 2025; Cin et al., 2026). However, such a comprehensive kinetic analysis has not yet been applied to $BaZr(BO_3)_2$.

Zirconium-containing borates and zirconates are of particular interest because Zr-centered complexes can act as efficient self-activated luminescence centers and may also participate directly in charge-transfer–based emission and trapping processes. For example, $K_2Zr(BO_3)_2$ exhibits self-activated cyan persistent luminescence, where TL deconvolution reveals four traps, the dominant one with a depth of ~0.66 eV responsible for room-temperature afterglow (Ju et al., 2017). Similarly, $Ba_2Zr_2Si_3O_{12}$ and $BaZrSi_3O_9$:Eu^{2+},Pr^{3+} display strong persistent luminescence whose mechanisms have been elucidated through TL-derived trap depth distributions (Guo et al., 2017; Xiong et al., 2020). TL kinetics of Eu^{3+}/Tb^{3+}-doped perovskite zirconates $AZrO_3$ (A = Ca, Sr, Ba) further demonstrate that Zr-based frameworks can host deep traps (~3 eV) with second-order recombination suitable for TL sensing applications (Katyayan and Agrawal, 2019). These studies collectively demonstrate that Zr-based frameworks provide efficient trapping–recombination environments and thus represent promising platforms for trap engineering in TL and persistent luminescence materials (Reddy et al., 2025).

To the best of our knowledge, $BaZr(BO_3)_2$ has not yet been systematically investigated using TL techniques, despite the fact that structurally related Ba-borate and Zr-borate hosts exhibit favorable dosimetric and persistent luminescence properties (Gavhane et al., 2020; Kumar and Bindu, 2022; Joseph et al., 2023; Salas-Juárez et al., 2023), and several other Zr-containing frameworks have already been analyzed using TL techniques (Encinas-Osuna et al., 2023; Gardenali Yukihara, 2023). The combination of Ba^{2+}, Zr^{4+}, and [BO_3] groups suggests a structurally robust, wide-band-gap host in which intrinsic defects and/or dopant-induced centers may form a tailored hierarchy of traps, potentially enabling both dosimetry and information-storage applications.

Given that TL analysis has played a central role in understanding modern TLD and persistent luminescence materials, investigating the TL behaviour of $BaZr(BO_3)_2$ may provide valuable insight into trap formation and recombination processes in Zr-containing borate frameworks.

To address this gap, a comprehensive TL investigation of $BaZr(BO_3)_2$ is undertaken. X-ray diffraction (XRD) is essential to confirm phase purity and to correlate crystal structure with trapping behaviour, in line with earlier TL work on borate and silicate hosts (Kucuk, 2019; Alshoaibi et al., 2023; Menezes et al., 2024). Dose-response measurements allow assessment of linearity, saturation, and suitability for low- and high-dose dosimetry, as demonstrated for $GdAl_3(BO_3)_4$, $YAl_3(BO_3)_4$:Sm^{3+}, LaB_3O_6:Nd^{3+}, $Ba_2Mg(BO_3)_2$:Tm^{3+} and related systems 121 820. Systematic heating-rate studies probe thermal quenching and possible anomalous heating-rate behaviour, which has been reported as a characteristic feature in several borate-based TL phosphors (Dogan et al., 2019; Nabadwip Singh, 2021; Szumera et al., 2022).

For practical applications, fading and reusability must be quantified. Many modern TL borate phosphors exhibit low signal loss over storage times of days to weeks and stable responses over multiple irradiation–readout cycles (Joseph et al., 2023; Ullah et al., 2024; Anishia et al., 2011). Establishing the temporal stability and cycle-to-cycle reproducibility of $BaZr(BO_3)_2$ is therefore a crucial step in evaluating its suitability as a dosimetric material.

Finally, rigorous trap-kinetic analysis using a comprehensive set of TL kinetic methods provides a detailed picture of the trapping landscape, including the number of traps, their depths and concentrations, kinetic order, and potential anomalous features. Applying this approach to $BaZr(BO_3)_2$ is particularly significant, as it enables direct comparison with state-of-the-art borate and zirconate TL phosphors, while revealing whether $BaZr(BO_3)_2$ supports discrete or distributed traps, general-order kinetics, and trap configurations favorable for dosimetry or persistent luminescence.

In this context, the present work reports the first systematic investigation of the TL properties and trap kinetics of $BaZr(BO_3)_2$, combining structural characterization, dosimetric evaluation, and comprehensive kinetic analysis (VHR, IR, T_m–T_{stop}, and GCD) to elucidate its trapping mechanisms and assess its suitability as a potential TL phosphor for radiation dosimetry.

2. Materials and methods

2.1. Synthesis of $BaZr(BO_3)_2$ phosphor

$BaZr(BO_3)_2$phosphor was synthesized via a microwave-assisted sol–gel auto-combustion method. In the synthesis process, high-purity zirconium (IV) oxynitrate hydrate ($ZrO(NO_3)_2{\cdot}xH_2O$, Merck, ≥99.0%), barium nitrate ($Ba(NO_3)_2$, Sigma-Aldrich, ≥99.5%), and boric acid (H_3BO_3) were used as oxidizing agents. A mixture of urea and glycine served as the fuel in the combustion process. All chemicals were precisely weighed according to the reaction stoichiometry before being introduced into the synthesis medium.

In the first stage of the synthesis, the required precursor materials were placed in a quartz beaker and dissolved in 20 mL of ultrapure water. Afterward, urea and glycine were added as fuels, and the solution was covered with a watch glass and stirred using a magnetic stirrer at 80 °C for 1 h to obtain a homogeneous mixture. The solution was then continuously stirred at the same temperature until it reached a gel-like consistency, allowing the excess water to evaporate.

The resulting gel was transferred to a microwave oven (850 W). After several minutes of microwave irradiation, the gel underwent a rapid self-propagating combustion reaction accompanied by intense gas evolution. As a result of this reaction, a foamy and highly porous white precursor powder was obtained (Chen et al., 2009). To complete the combustion process and eliminate possible organic residues, the obtained samples were annealed at 920 °C for 4 h (Deng et al., 2024). After the heat treatment, crystalline $BaZr(BO_3)_2$vnanostructures were successfully obtained. The synthesized samples were stored in a desiccator to prevent moisture absorption until further characterization analyses were performed.

Such a microwave-assisted sol–gel auto-combustion route, employing metal nitrates and urea-based fuels for the synthesis of nanostructured Ba–Zr–O based ceramics, has been widely reported in the literature for $BaZrO_3$ and related oxide systems (Manju et al., 2019; Junliang et al., 2010). Moreover, microwave-assisted sol–gel auto-combustion methods using nitrate–urea fuel systems have been successfully applied for the rapid synthesis of Ba-containing oxide and hexaferrite nanopowders (Castro et al., 1996; Roy et al., 2021). In addition, previous studies have shown that microwave heating can facilitate the formation of Zr–B based ceramic precursors at relatively lower temperatures, highlighting the effectiveness of microwave-assisted synthesis routes (Ding et al., 2021).

2.2. Material characterization

X-ray diffraction (XRD) measurements were carried out to determine the phase composition and structural characteristics of $BaZr(BO_3)_2$. The diffraction patterns were recorded using a PANalytical Empyrean diffractometer (Malvern PANalytical) with Cu Kα radiation (λ = 1.5406 Å). Data were collected over a 2θ range of 10°–80° to ensure

reliable phase identification.

TL measurements were performed using a Lexsyg Smart TL/OSL reader (Freiberg Instruments, Germany), equipped with an internal $^{90}Sr/^{90}Y$ β radiation source providing a nominal dose rate of approximately 1.436 Gy s^{-1}. All TL experiments were conducted at Bakırçay University. Prior to measurements, nearly 23 mg of $BaZr(BO_3)_2$ powder was uniformly mixed and pressed into pellets with a diameter of 6 mm using a manual hydraulic press to obtain stable sample geometry and improved thermal contact during heating.

Following irradiation, TL glow curves were recorded by heating the samples from room temperature up to 450 °C under a linear heating regime. A heating rate of 2 °C s^{-1} was used to obtain the reference glow

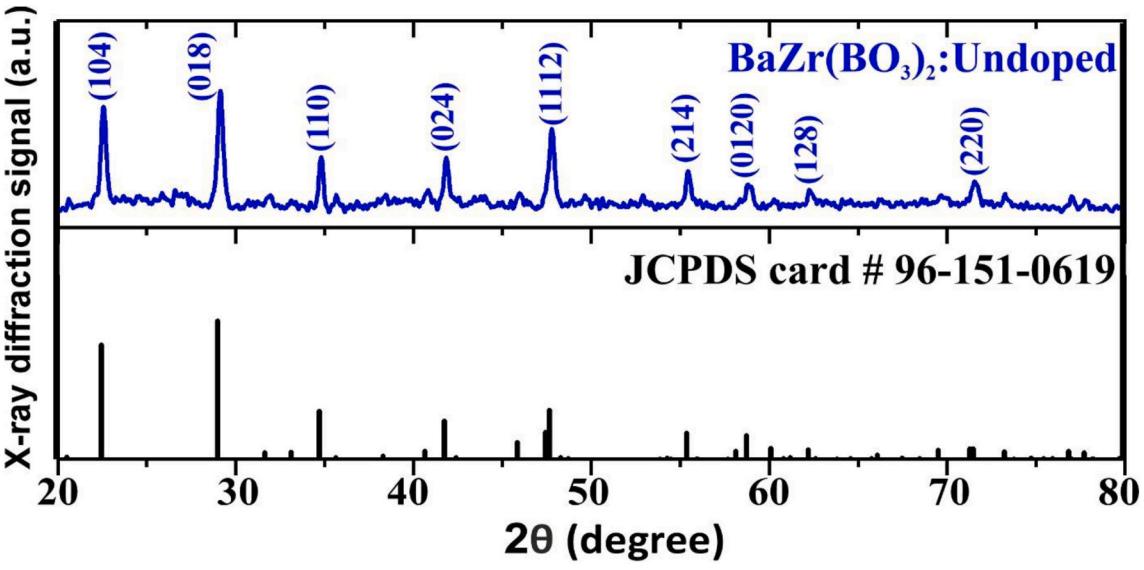

(a)

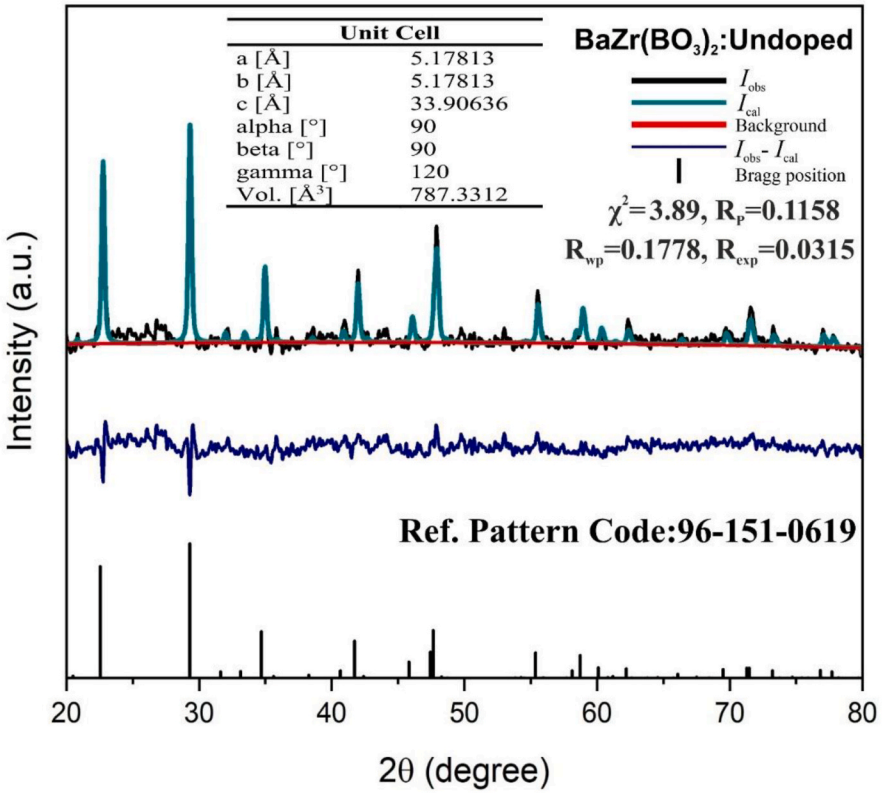

(b)

Fig. 1. (a) X-ray diffraction (XRD) pattern of the synthesized $BaZr(BO_3)_2$ phosphor. All diffraction peaks are indexed according to the standard reference pattern (JCPDS card No. 96-151-0619), confirming the formation of single-phase $BaZr(BO_3)_2$ with trigonal crystal structure (space group R3c). (b) Rietveld refinement of the XRD pattern of $BaZr(BO_3)_2$ phosphor. The observed intensities (open circles), calculated profile (solid line), and difference curve (bottom line) are presented along with the Bragg reflection positions.

curves. During the readout stage, the measurements were carried out under a continuous nitrogen flow in order to suppress oxidation and minimize possible chemiluminescence effects.

3. Results and discussions

3.1. Structural characterization by XRD

The X-ray diffraction (XRD) pattern of the synthesized $BaZr(BO_3)_2$ phosphor is presented in Fig. 1a. All diffraction peaks can be indexed according to the standard reference pattern (JCPDS card No. 96-151-0619), confirming the successful formation of the $BaZr(BO_3)_2$ phase without detectable impurity phases. The major reflections located at $2\theta \approx 23°$, 28°, 34°, 42°, 48°, 56°, 58°, 62°, and 72° correspond to the crystallographic planes (104), (018), (110), (024), (112), (214), (120), (128), and (220), respectively. $BaZr(BO_3)_2$ crystallizes in a trigonal structure with space group R3c as reported in previous crystallographic studies (Hornebecq et al., 2002; Mączka et al., 2015). No additional diffraction peaks are observed, indicating the formation of a single-phase material with good crystallinity. The absence of secondary phases suggests that the observed TL properties originate from intrinsic trapping centers within the undoped $BaZr(BO_3)_2$ host lattice, consistent with the intrinsic TL behaviour discussed in this work. The dolomite-type layered arrangement of corner-sharing BaO_6 and ZrO_6 octahedra interconnected by BO_3 groups is expected to facilitate the formation of intrinsic point defects that can act as trapping centers relevant for the observed TL response (Leon et al., 2024). Such polyhedral frameworks in borate hosts are known to promote defect-related trapping processes that strongly influence TL behaviour.

Fig. 1b shows the Rietveld refinement of the XRD pattern of $BaZr(BO_3)_2$ phosphor. The observed intensities, calculated profile, and difference curve are presented together with the Bragg reflection positions. All reflections are well reproduced by the calculated pattern, confirming the trigonal *R3c* structure and the absence of secondary phases. The refinement converged with reliability factors of $R_p = 0.1158$, $R_{wp} = 0.1778$, and $\chi^2 = 3.89$, indicating a satisfactory agreement between the experimental and calculated profiles. The absence of systematic deviations in the difference curve further supports the high phase purity and good crystallinity of the sample.

The refined lattice parameters ($a = b = 5.178$ Å, $c = 33.906$ Å) are in good agreement with the reference data (JCPDS 96-151-0619), confirming the validity of the structural model used in the refinement. The Rietveld refinement was performed using a pseudo-Voigt profile function with a polynomial background model, ensuring reliable fitting of peak shapes and background contribution.

3.2. Experimental optimization of TL readout conditions

3.2.1. Optical filter selection

The TL glow curves of $BaZr(BO_3)_2$ recorded using different optical filters are shown in Fig. 2a. TL spectra were acquired using the standard detection filter configurations of the Lexsyg Smart reader. In the UV-sensitive setup (BSL–TL 365 nm), a U-340 glass filter in series with a BP365/50 interference filter was used, defining a detection band of roughly 340–390 nm while strongly blocking visible and infrared photons. The blue-sensitive configuration (IRSL–TL 410 nm) combined a BG-39 glass filter with an HC414/46 interference filter, giving a response centered at about 410–415 nm with an effective transmission range of approximately 390–440 nm. For green-sensitive detection (IRSL–TL 565 nm), BG-39 was paired with an HC575/25 interference filter, restricting the signal to about 565–580 nm and efficiently suppressing contributions from UV/blue as well as red/IR wavelengths. A broad-band blue detection option (BG39 + BG25 + KG3) is available for wide-range TL/IRSL measurements but was excluded from the present kinetic study. Comparable filter arrangements and their dosimetric use have been described for $Ca_3Al_2O_6$ phosphors, where they enabled separation of UV, blue, and green emission components (Bakr et al., 2020). Noticeable variations in both intensity and the apparent positions of the glow peaks are observed depending on the selected wavelength window. These differences originate from wavelength-selective detection of luminescence; however, in the framework of modern thermoluminescence models, such spectral variations may also reflect coupling

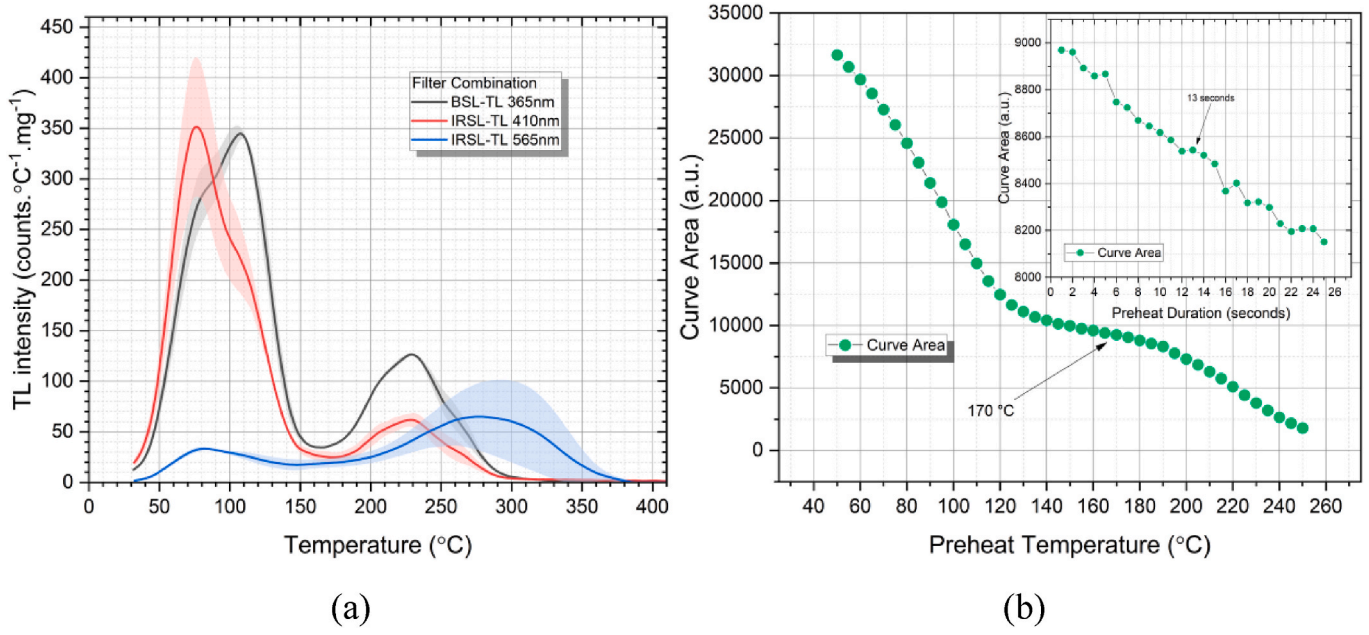

Fig. 2. TL characteristics of $BaZr(BO_3)_2$ phosphor irradiated at 50 Gy: (a) TL glow curves recorded using different optical filters. The mean net signal from three measurements for each combination is shown, with the corresponding standard deviation values represented as deviation bands; (b) dependence of the integrated TL curve area on preheating temperature. The preheating protocol consisted of heating at 2 °C/s to 170 °C, holding for 13 s, and subsequently cooling to room temperature before TL measurement. The inset shows a representative TL glow curve obtained after preheating, demonstrating the isolation of the stable high-temperature peak.

between trapping and recombination centers Optical filters restrict the detected emission to specific spectral regions and therefore emphasize different radiative recombination pathways associated with distinct emission centers. In systems where traps and recombination centers form closely associated defect complexes, such wavelength-selective detection can preferentially probe different local configurations, leading to observable variations in both emission intensity and glow-peak characteristics.

Among the tested filters, the 365 nm filter produced the highest TL intensity and the most clearly resolved glow peaks, allowing both the low-temperature (~76 °C) and high-temperature (~226 °C) components to be monitored effectively. In contrast, the 565 nm filter significantly suppresses the low-temperature emission, indicating that this recombination channel contributes weakly within the red spectral region. The filter-dependent variations in peak appearance therefore suggest the presence of multiple emission or recombination centers contributing to the overall TL signal. Based on the superior signal intensity and peak resolution, the 365 nm filter was selected as the detection window for all subsequent TL measurements.

In addition to the intensity variations, slight shifts in the apparent peak positions are observed depending on the selected optical filter. Although the optical filter itself does not alter the intrinsic defect population, the observed shifts in the apparent peak positions indicate that different emission bands are associated with different recombination centers. In the presence of trap–recombination coupling, these centers may slightly modify the effective activation energy, resulting in filter-dependent variations in the apparent peak temperature. Different spectral windows emphasize different recombination centers, and

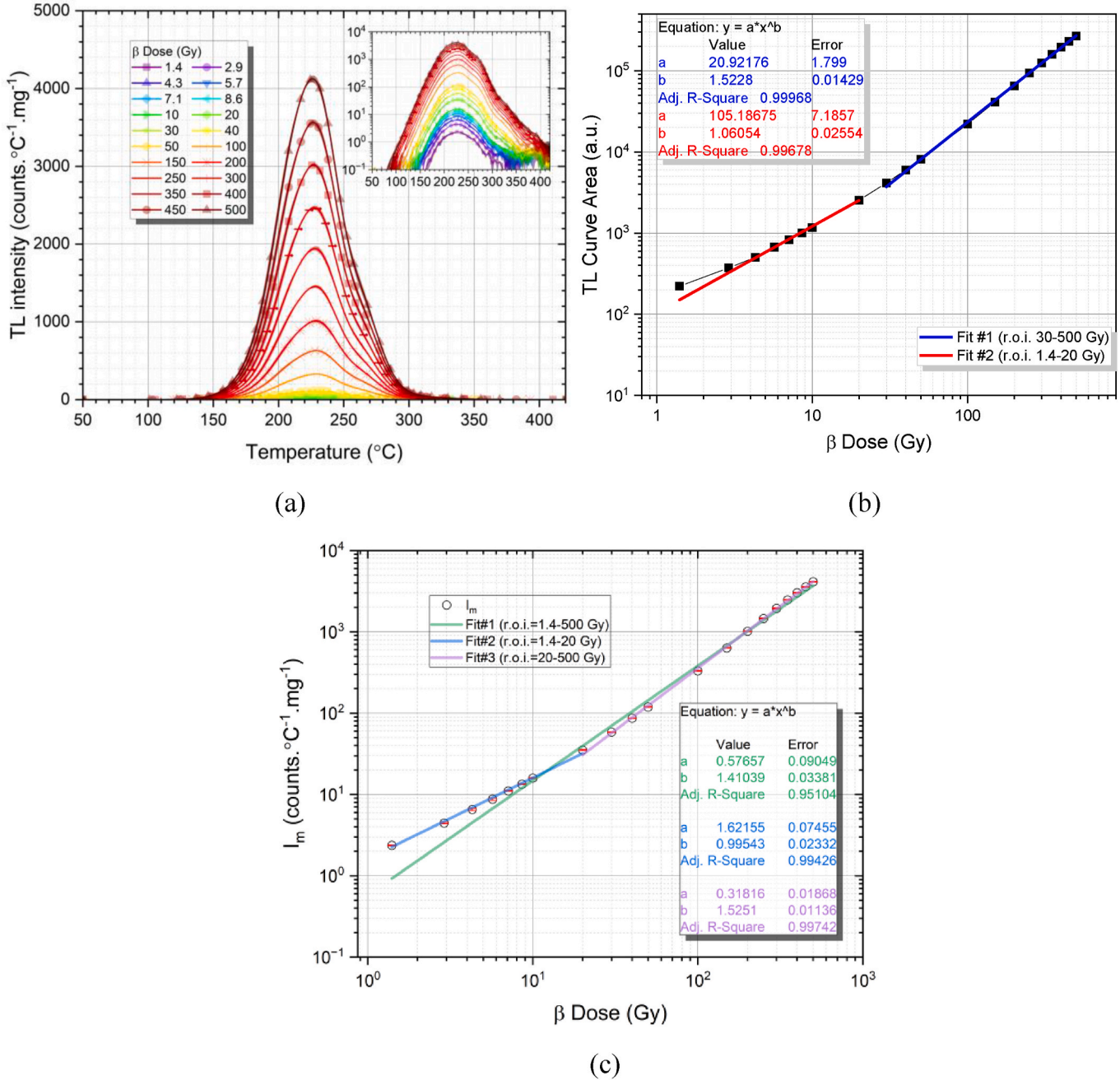

Fig. 3. TL dose–response characteristics of $BaZr(BO_3)_2$ phosphor: (a) TL glow curves recorded at different β irradiation doses, with the mean net signal obtained from three measurements for each dose level. The inset shows a semi-logarithmic representation to highlight the low-dose glow curves, (b) dose dependence of the integrated TL glow-curve area, and (c) dose dependence of the peak intensity.

therefore overlapping TL components can appear at slightly different temperatures depending on the detected emission band. Such filter-dependent peak variations have been reported previously in TL phosphors where multiple recombination pathways contribute to the glow curve. Such filter-dependent variations in both intensity and apparent peak position have been widely reported in thermoluminescent materials and are commonly interpreted as evidence of coupling between trapping and recombination sites within defect complexes, as discussed in the literature (Townsend et al., 2021; McKeever, 2025).

3.2.2. Optimization of the preheating temperature

The preheating temperature was optimized by monitoring the variation of the integrated TL curve area as a function of preheat temperature, as presented in Fig. 2b. As the preheating temperature increases, the total TL area decreases rapidly at lower temperatures due to the progressive thermal release of charge carriers from shallow and thermally unstable traps. At higher temperatures the curve approaches a plateau region around 170 °C, indicating that the unstable shallow trapping contribution has been largely removed while the deeper trapping centers remain preserved.

Additional short-term storage tests (not shown) revealed that the low-temperature TL peak exhibits significant fading, losing nearly 80% of its intensity after 12 h of storage, confirming its unstable nature. Therefore, based on the preheating dependence shown in Fig. 2b, a preheating condition of 170 °C for 13 s was selected to suppress the unstable low-temperature component and to isolate the stable high-temperature dosimetric peak. The inset of Fig. 2b presents a representative TL glow curve after preheating, confirming that the resulting signal is dominated by a single stable peak suitable for subsequent TL and kinetic analyses.

3.3. Dose-response behaviour of the TL glow curve

The TL glow curves recorded at different β irradiation doses are shown in Fig. 3a. As the irradiation dose increases from 1.4 Gy to 500 Gy, the TL intensity increases systematically, while the peak maximum temperature ($T_m \approx 226$ °C) remains nearly unchanged. Such behaviour indicates that the underlying trapping parameters, including the activation energy and frequency factor, remain essentially constant with increasing dose (Pagonis and Kitis, 2012; Chen, 1969; Kitis and Pagonis, 2017).

In TL processes, increasing dose primarily increases the number of filled traps without significantly modifying the trap structure or recombination probability. Consequently, the TL intensity increases due to the release of a larger number of trapped charge carriers during thermal stimulation, whereas the temperature corresponding to the maximum release rate (T_m) remains nearly constant (Kalita and Chithambo, 2017).

The absence of a significant peak shift together with the preservation of the glow-curve shape suggests that the dominant trapping–recombination process behaves close to first-order kinetics, where retrapping effects are relatively weak and the trap population remains far from saturation. Such dose-independent T_m behaviour has been widely reported in established TL dosimetric materials (Oguntona and Ogundare, 2019; Sunta et al., 1998). In contrast, theoretical simulations and experimental studies of strong retrapping or second-order kinetics predict a dose-dependent shift of T_m, typically toward lower temperatures as trap filling increases (Tsoutsoumanos et al., 2022; Sadek et al., 2015). The absence of such a shift in the present study therefore further supports the predominance of near first-order TL kinetics in $BaZr(BO_3)_2$.

To further evaluate the dosimetric characteristics of the material, the dose–response behaviour was analyzed using two TL response parameters: the integrated glow-curve area and the maximum peak intensity. The dose dependence of the integrated TL signal is presented in Fig. 3a, where the response was fitted using a power-law relation of the form $y = ax^b$. The exponent b provides information about the linearity of the response (Yamazaki et al., 1978). In the low-dose interval (approximately 1.4–20 Gy), the fitted b value is close to unity, indicating that the dose response approaches linear behaviour in this region. The integrated glow-curve area shows near-linear behaviour up to about 20 Gy, suggesting that the total TL emission is approximately proportional to the number of filled traps within this dose interval.

At higher doses (approximately 30–500 Gy), the integrated TL response begins to deviate from strict linearity and exhibits a supralinear trend, as indicated by the increase in the fitted exponent b (~1.50). This behaviour suggests that additional trapping or recombination processes become progressively involved as the trap population increases. Such supralinear dose dependence is commonly attributed to trap competition, the activation of deeper trapping centers, or changes in the recombination probability as the trap occupancy increases. Nevertheless, the TL signal continues to increase monotonically with dose throughout the investigated high-dose range, indicating that trap saturation has not yet been reached within this interval.

For comparison, the dose response based on the peak height is shown in Fig. 3b and c. In this case, the response shows near-linear behaviour at low doses (~1.4–10 Gy), followed by a gradual deviation at higher doses. The fitted exponent b becomes larger than unity at higher doses, indicating the onset of supralinear behaviour. Such differences between peak-height and area-based dose evaluation are commonly observed in TL materials, since the peak height can be more sensitive to subtle changes in glow-curve width or shape at higher doses.

Overall, the comparison of Fig. 3b and c indicates that both the integrated TL glow-curve area and the peak-height methods show a similar dose dependence in the low-dose interval (~1.4–20 Gy), without implying a strictly segmented linear behaviour. The peak-height response remains closer to ideal linearity ($b \approx 1.00$), whereas the integrated area exhibits a slight deviation ($b \approx 1.06$). At higher doses, both parameters display a gradual supralinear trend ($b \approx 1.5$). These results suggest that neither method provides a significantly wider low-dose region with near-linear response; however, the integrated TL area remains the more robust parameter, as it reflects the total emitted signal over the entire glow curve (Halefoglu et al., 2020; Liuzzi et al., 2020). Dose–response behaviour in thermoluminescent materials is more appropriately described as a continuous function rather than as a sum of discrete linear regions, as discussed in the literature (ChenR, 2011).

The detection limit of the $BaZr(BO_3)_2$ dosimeter was quantified using the conventional expression for the minimum detectable dose (MDD) (Pagonis et al., 2006):

$$D_{LDL} = 3\sigma_{Bkg}\Phi_c \quad (1)$$

where (σ_{Bkg}) is the standard deviation of the mean background signal obtained from non-irradiated pellets, and (Φ_c) is the calibration factor, defined as the ratio between the applied dose (Gy) and the corresponding net TL signal at that dose. Using this formalism, an MDD value of (117.57 ± 1.91 mGy}) was obtained for the main dosimetric peak under the optimized readout conditions (365 nm window, preheat at 170 °C).

The calculated MDD lies in the sub-hundred milligray range, which is typically considered suitable for routine environmental and clinical dosimetry. This value is consistent with the performance reported for several borate-based TL phosphors, although a direct quantitative comparison is not possible due to the lack of uniformly reported MDD and low-dose linearity data across the literature. Borate hosts such as rare-earth-doped lithium and zinc borates, including $Li_2B_4O_7$:Cu, Ag (Ullah et al., 2024), have demonstrated low-dose detection capability with a linear or near-linear dose response in the low-dose region, while materials such as $LaCa_4O(BO_3)_3$:Tb^{3+} (Madkhali et al., 2025) exhibit high sensitivity with more complex (superlinear-to-linear) dose-response behaviour. In this context, the present MDD result indicates that $BaZr(BO_3)_2$ can resolve small dose increments within its linear dose-response interval and suggests that it is a promising

candidate for low-dose TL dosimetry, in line with other borate and zirconate hosts proposed for such applications.

3.4. Reusability of the TL signal

The reusability of the TL signal is an important parameter for evaluating the practical applicability of TL materials in radiation dosimetry. To investigate the stability and reproducibility of the TL response, repeated irradiation–readout cycles were performed under identical experimental conditions. The reusability test was carried out over 15 successive irradiation–readout cycles under identical measurement conditions.

The TL glow curves obtained from successive measurement cycles are presented in Fig. 4a. The curves nearly coincide with each other, indicating that the overall glow-curve shape and the peak position remain essentially unchanged during repeated measurements. This behaviour suggests that the trapping and recombination processes in the material are stable and are not significantly affected by repeated irradiation and thermal readout.

For a more quantitative evaluation, the TL signal corresponding to the maximum glow-peak intensity was normalized to the first measurement and plotted as a function of the readout cycle number, as shown in Fig. 4b. The normalized TL intensities remain close to unity throughout the repeated cycles, with all data points lying within the 95% confidence interval. The variation of the TL response remains within a narrow range of approximately ±3–5%, indicating good cycle-to-cycle reproducibility (Del Sol Fernández et al., 2016). The small fluctuations observed between cycles are within the expected experimental uncertainty and do not indicate any systematic sensitivity loss or gain. In addition, the reusability behaviour was further evaluated using the integrated TL glow-curve area, as shown in Fig. 4c. The normalized curve-area values also remain close to unity over all measurement

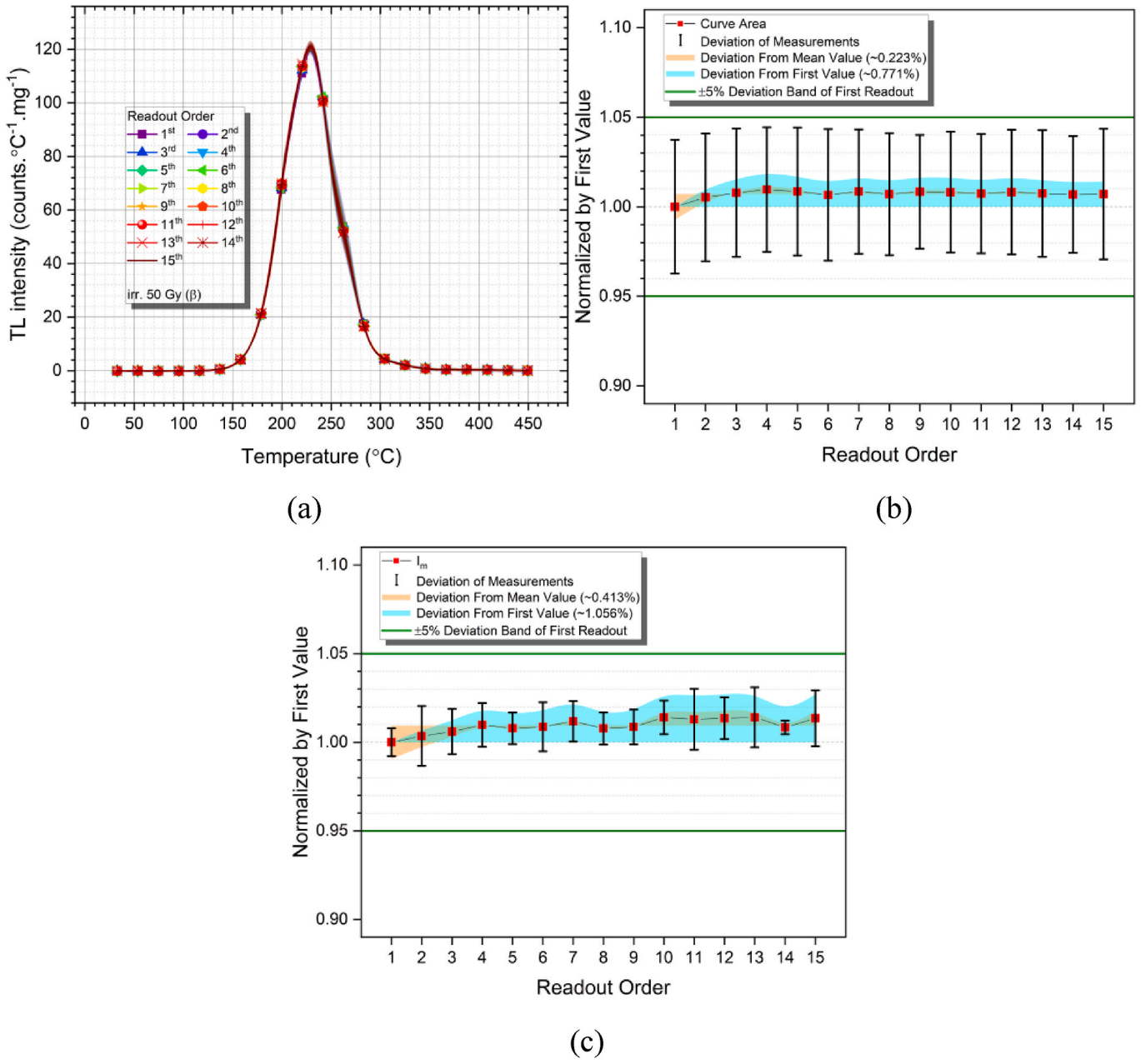

Fig. 4. Reusability test of $BaZr(BO_3)_2$ phosphor: (a) TL glow curves recorded over repeated irradiation–readout cycles; (b) normalized TL peak intensity (I_m) as a function of readout cycle; (c) normalized integrated TL glow-curve area as a function of readout cycle.

cycles, with deviations comparable to those observed for the peak intensity. This consistency between peak-height and integrated-area analyses confirms that both parameters exhibit stable and reproducible responses under repeated irradiation–readout conditions.

The observed cycle-to-cycle stability is consistent with that reported for several borate-based TL phosphors used in radiation dosimetry, which exhibit stable responses over repeated irradiation–readout cycles. These results demonstrate that the studied phosphor exhibits good cycle-to-cycle reusability and readout stability, which are essential characteristics for reliable TL dosimetric applications.

3.5. Heating rate dependence and temperature lag correction

The influence of the heating rate on the TL glow curve of $BaZr(BO_3)_2$ was investigated in the range of 0.1–5 °C s^{-1}, and the resulting glow curves are presented in Fig. 5a. As the heating rate increases, the TL peak maximum shifts systematically toward higher temperatures while the overall glow-curve structure remains similar. This behaviour is

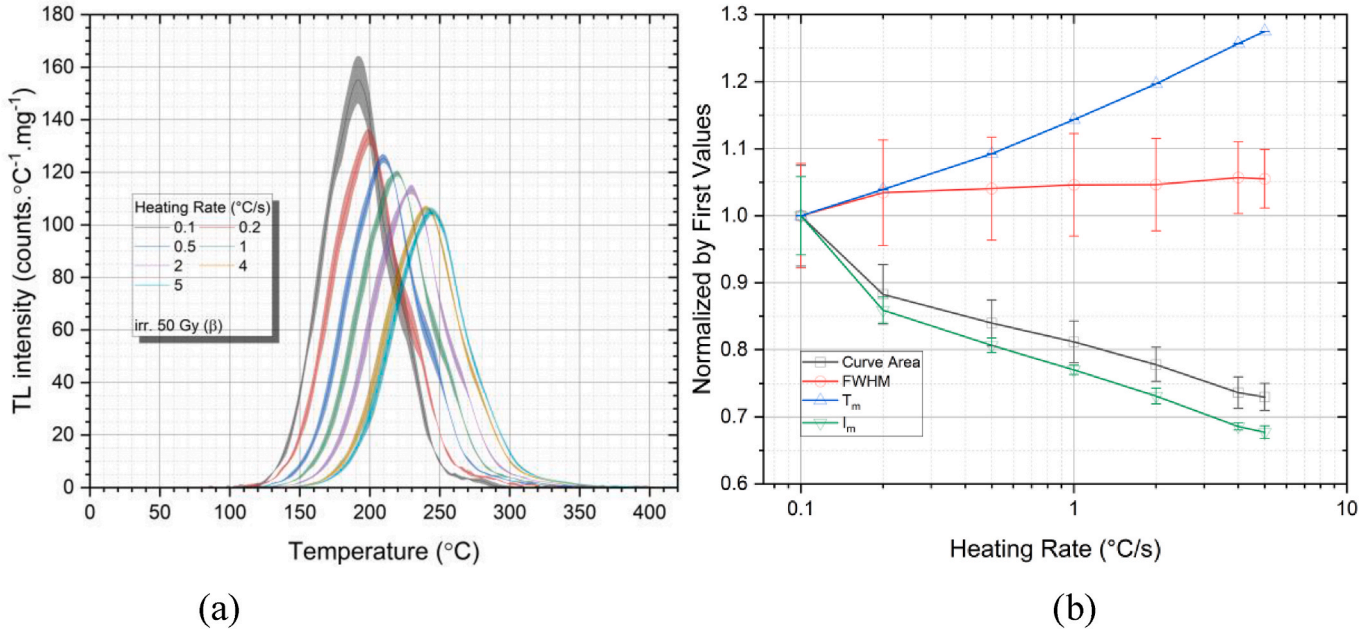

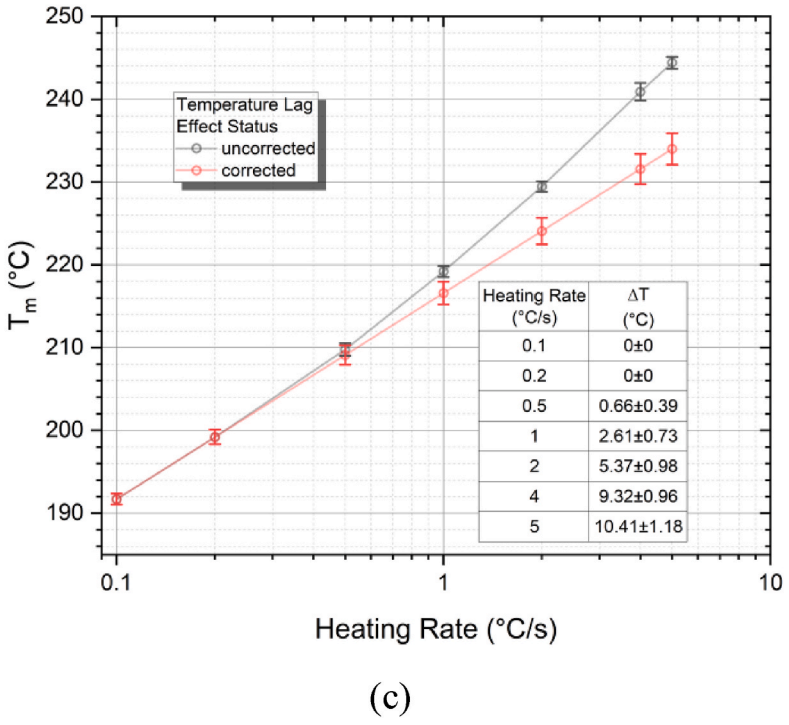

Fig. 5. (a) TL glow curves of $BaZr(BO_3)_2$ recorded at heating rates of 0.1–5 °C s^{-1} after β irradiation (50 Gy) using a 365 nm filter and preheating at 170 °C for 13 s. The dominant peak (~226 °C) shifts to higher temperatures with increasing heating rate. (b) Dependence of glow-curve shape parameters on heating rate. (c) Peak temperature (T_m) as a function of heating rate before and after temperature-lag correction.

commonly observed in TL materials and arises because faster heating reduces the time available for thermal release of trapped charge carriers, requiring higher temperatures to reach the maximum recombination rate.

The variation of the glow-curve shape parameters with heating rate is summarized in Fig. 5b, where the symmetry factor and related peak-shape parameters are plotted as a function of the heating rate. The systematic variation of these parameters reflects the influence of heating rate on the apparent glow-curve profile and provides useful information for subsequent kinetic analysis.

However, when TL measurements are performed at different heating rates, the measured peak temperature (T_m) can be affected by temperature lag between the sample and the heater. In a linear heating experiment, finite thermal contact and limited heat transfer cause the sample temperature to lag behind the heater temperature, and this lag increases with increasing heating rate. To account for this effect, a temperature lag correction was applied using Eq. (2) (Kitis and Tuyn, 1998):

$$T_{m_j} = T_{m_i} - \frac{T_{m_2} - T_{m_1}}{ln\left(\frac{\beta_2}{\beta_1}\right)} ln\left(\frac{\beta_i}{\beta_j}\right) \quad (2)$$

where β represents the heating rate and Tm corresponds to the peak temperature obtained at a given heating rate. The corrected and uncorrected peak temperatures are compared in Fig. 5c. The inset in Fig. 5c illustrates the magnitude of the temperature lag observed at different heating rates, where the shift in T_m increases from approximately 0.44 °C at 0.5 °C s^{-1} to about 8.09 °C at 5 °C s^{-1}. After applying this correction, the resulting T_m values were used in the VHR analysis to determine the kinetic parameters of the dominant TL peak. If this effect is neglected, the apparent peak temperatures may be artificially shifted, which can lead to an underestimation of the activation energy in variable heating rate analyses.

4. Kinetic characterization

4.1. Variable heating rate (VHR) approaches for activation energy estimation

The trap depth associated with the dominant TL peak was evaluated using several approaches based on the VHR technique. These methods rely on the systematic displacement of the glow-peak maximum temperature (T_m) as the linear heating rate (β) is varied. By analyzing this temperature shift, the kinetic parameters of the trapping centers can be determined without performing a full deconvolution of the glow curve.

(i) Hoogenstraaten Method

One of the classical VHR approaches is the method introduced by Hoogenstraaten (1958), which relates the heating rate to the peak temperature through a linear expression involving the quantities ln (T_m^2/β) and $1/T_m$. When these parameters are plotted against each other, a straight line is obtained whose slope is proportional to the activation energy *E*, while the intercept provides an estimate of the frequency factor *s*.

Although the derivation of this method assumes first-order kinetics, subsequent investigations have demonstrated that it can also yield reasonable estimates of the activation energy for glow peaks following general-order kinetics or more complex recombination mechanisms. Consequently, the Hoogenstraaten approach remains widely used for preliminary evaluation of trap depths in TL studies.

(ii) Booth–Bohun–Parfianovitch (Two-Rate) Method

An alternative VHR-based procedure is the Booth–Bohun–Parfianovitch (BBP) method (Booth, 1954; Bohun, 1954; Parfianovitch, 1954), which utilizes only two heating rates to estimate the activation energy. In this approach, the activation energy is calculated from the temperatures of the same TL peak measured at two different heating rates according to

$$E_a = k\frac{T_{m_1}T_{m_2}}{T_{m_1} - T_{m_2}} ln\left[\frac{\beta_1}{\beta_2}\left(\frac{T_{m_2}}{T_{m_1}}\right)^2\right] \quad (3)$$

where T_{m1} and T_{m2} are the peak temperatures corresponding to heating rates β_1 and β_2 , respectively, and *k* is the Boltzmann constant.

Because this method requires only two measurements, it offers a rapid and convenient means of estimating trap depths. Previous studies have shown that, when appropriate heating-rate pairs are selected, the two-rate method can provide reliable kinetic parameters even for TL peaks that follow general-order kinetics.

(iii) Gartia et al. (1991) Method

Gartia et al. proposed a VHR-based approach by combining numerical simulations with experimental TL data, expressed as (Gartia et al., 1991):

$$E = k\frac{T_{m_1}T_{m_2}}{T_{m_1} - T_{m_2}} ln\left[\left(\frac{I_{m_1}}{I_{m_2}}\right)\right] \quad (4)$$

Their analysis examined the influence of kinetic order and peak parameters on the accuracy of the extracted activation energies and demonstrated that commonly used VHR variants, including Hoogenstraaten-type formulations, can provide reliable activation energy estimates that are largely independent of the assumed kinetic model under realistic TL conditions (Gartia et al., 1991).

Fig. 6 presents the corresponding Hoogenstraaten plot obtained from the relationship between ln (T_m^2/β) and $1/T_m$ using both the temperature-lag–corrected and uncorrected peak temperatures. In both cases, the data points exhibit a good linear correlation, indicating that the temperature shift of the glow-peak maximum with heating rate follows the expected behaviour for thermally activated charge release.

From the slope of the fitted lines, the activation energy values were determined as 1.452 ± 0.036 eV for the uncorrected data and 1.734 ± 0.019 eV after applying the temperature-lag correction as shown in Table 1. The corresponding frequency factors obtained from the intercepts were 5.004×10^{13} s^{-1} and 9.094×10^{15} s^{-1}, respectively, which fall within the typical range reported for deep TL traps in oxide

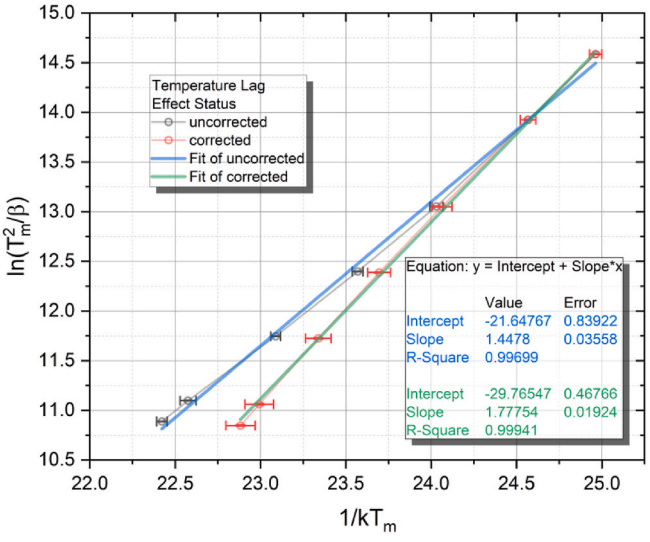

Fig. 6. Hoogenstraaten plot showing the relationship between ln (T_m^2/β) and $1/T_m$ for the dominant TL peak of $BaZr(BO_3)_2$.

Table 1
Activation energies of the dominant TL peak of $BaZr(BO_3)_2$ obtained using the Hoogenstraaten, Booth–Bohun–Parfianovitch (BBP), and Gartia et al. methods; the Hoogenstraaten frequency factor (*s*) is also reported. Results based on both corrected and uncorrected T_m values are presented.

Calculated Effective E_a (eV)			
β (°C/s)	Temp. Lag Effect Status		Method
	Uncorrected	Corrected	
Average of Pairs of 0.1 to 5	1.42 ± 0.12	1.82 ± 0.12	Booth-Bohun-Parfianovitch Method (Parfianovitch, 1954)
0.1 to 5	1.45 ± 0.04	1.78 ± 0.02	Hoogenstraaten's Method (Hoogenstraaten, 1958)
Average of Pairs of 0.1 to 5	1.39 ± 0.10	1.73 ± 0.13	Gartia et al. (Gartia et al., 1991)

and borate phosphors and are consistent with a thermally stable trapping center (Alathlawi et al., 2025; Chandrasekhar, 2025). These results clearly demonstrate that neglecting the temperature lag leads to an underestimation of the trap depth. After correction, the obtained activation energy falls within the typical range reported for TL trapping centers in oxide and borate hosts (Daniel et al., 2019; Sonsuz et al., 2022).

In BBP approach, the T_m values corresponding to different heating rates were paired with each other and the activation energy was calculated for each heating-rate combination. The resulting values were then averaged to obtain the representative activation energy for the investigated TL peak.

Table 1 summarizes the activation energy values obtained using both the corrected and uncorrected peak temperatures. The average activation energies derived from the BBP method were 1.263 ± 0.048 eV and 1.504 ± 0.039 eV for the uncorrected and corrected datasets, respectively. As observed in the Hoogenstraaten analysis, the application of the temperature-lag correction systematically increases the estimated trap depth, confirming the importance of accounting for this effect in heating-rate-based kinetic analyses.

To further validate the VHR analysis, activation energies were also evaluated using the approach proposed by Gartia et al. (1991), which accounts for the influence of kinetic order and peak-shape parameters. The activation energy values obtained using this method ($E_a \approx 1.39 \pm 0.10$ eV uncorrected and 1.73 ± 0.13 eV corrected) are in good agreement with those derived from the Hoogenstraaten and BBP methods (Table 1). This consistency indicates that the estimated trap depth is largely independent of the specific VHR formulation and supports the reliability of the kinetic analysis.

Overall, the activation energy values obtained from the Hoogenstraaten, BBP, and Gartia approaches are in reasonable agreement and indicate that the dominant TL peak of $BaZr(BO_3)_2$ is associated with a deep trapping center suitable for stable TL emission.

4.2. Kinetic diagnostics using initial rise and T_m–T_{stop} methods

The trapping structure of the investigated phosphor was further examined using the combined IR and T_m–T_{stop} approaches. These methods provide diagnostic insight into the energetic distribution of trapping centers without requiring the assumption of a specific global kinetic model (Pagonis et al., 2014; McKeever, 1980).

Under linear heating conditions, the glow-peak maximum temperature (T_m) reflects the temperature at which the thermal release rate of trapped carriers becomes comparable to the applied heating rate. Consequently, the position of T_m is closely related to the activation energy of the trap and the probability of carrier escape.

In the T_m–T_{stop} procedure, the sample is first irradiated and then preheated to a selected stop temperature (T_{stop}). After rapid cooling, the remaining TL signal is recorded during a complete readout. By progressively increasing T_{stop}, carriers stored in shallower traps are selectively emptied, allowing deeper trapping levels to dominate the subsequent glow curve. For materials containing discrete trapping levels, this procedure typically produces plateau regions in the T_m–T_{stop} relationship, whereas systems with overlapping or distributed traps tend to exhibit a more gradual variation of T_m with increasing T_{stop} (Balci-Yegen et al., 2018; Wazir-ud-Din et al., 2023).

The IR method was applied to the low-temperature side of the glow peaks, where the TL intensity follows an exponential dependence of the form

$$I(T) \propto exp(-E_a / kT) \tag{5}$$

In this temperature region the probability of retrapping is relatively small, allowing the activation energy to be estimated from the slope of the Arrhenius-type relation (Kaynar et al., 2023). However, when the glow curve contains overlapping peaks or a distribution of traps, the obtained activation energy should be regarded as an effective value representing the dominant traps contributing within the analyzed temperature interval.

After progressively increasing the preheat temperature, the

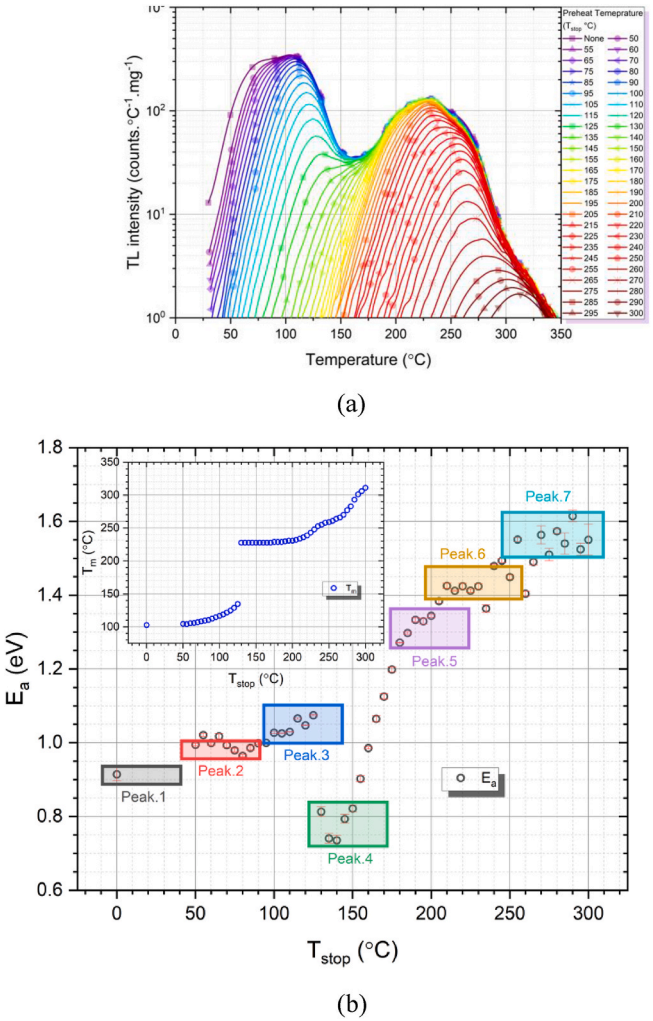

Fig. 7. (a) TL glow curves of $BaZr(BO_3)_2$ recorded after progressive preheating to different T_{stop} temperatures, illustrating the gradual removal of shallow traps. (b) Corresponding T_m–T_{stop} plot derived from these glow curves, showing a plateau region between ~130 and 200 °C associated with the dominant trapping level. The inset in (b) presents the variation of T_m as a function of T_{stop} in detail.

evolution of the TL glow curves is presented in Fig. 7a. As the stop temperature increases, the intensity of the low-temperature peak decreases rapidly and eventually disappears, indicating that the corresponding shallow trapping centers are thermally unstable and are progressively emptied during the preheating stage. In contrast, the high-temperature peak persists over a wider temperature interval, confirming the presence of deeper and more thermally stable trapping levels.

The corresponding T_m–T_{stop} relationship derived from these glow curves is shown in Fig. 7b. The inset in Fig. 7b provides a clearer representation of the T_m–T_{stop} variation, allowing a more precise identification of distinct regions. At low stop temperatures, T_m increases gradually as shallow traps are progressively removed and deeper traps begin to dominate the glow curve. More specifically, three characteristic regions can be distinguished: an initial increase in T_m between ~50 and 125 °C, a well-defined plateau region between ~125 and 200 °C, and a subsequent increase at higher T_{stop} values. The plateau region indicates the presence of a dominant and thermally isolated trapping level controlling the main TL peak. In T_m–T_{stop} analysis, such plateau behaviour is generally considered evidence of a dominant, thermally isolated discrete trap operating under quasi-first-order kinetic conditions. Similar T_m–T_{stop} plateau regions attributed to isolated trapping levels have been reported in several TL materials, including $GdAlO_3$, $LaCa_4O(BO_3)_3$ and feldspar phosphors (Madkhali et al., 2025; Pagonis et al., 2014; Nolasco-Altamirano et al., 2025).

The three-region evolution observed in the T_m–T_{stop} curve (initial increase, plateau, and final increase) is characteristic of a hierarchical trap structure comprising shallow, intermediate, and deeper levels. In particular, the well-defined plateau between ~125 and 200 °C implies that, within this T_{stop} interval, the TL signal is governed by a single, thermally isolated trap, consistent with quasi-first-order behaviour commonly reported for oxide and borate phosphors.

At higher stop temperatures, T_m begins to increase again, suggesting that deeper or partially overlapping trapping levels start to contribute to the remaining TL signal (Benavente et al., 2020). Although Fig. 7b does not directly display individual glow peaks, the inset clearly illustrates the T_m–T_{stop} evolution, where the observed increase–plateau–increase trend is consistent with a hierarchical trapping structure comprising multiple shallow and deeper traps surrounding a single dominant dosimetric peak governing the TL signal within the plateau region.

The corresponding E_a–T_{stop} plot in Fig. 7b further supports this interpretation. The scattered and relatively low E_a values at small T_{stop} reflect the coexistence of multiple shallow and thermally unstable traps. In contrast, the nearly constant E_a values observed within the plateau region indicate the energetic uniformity of the dominant trap controlling the main TL peak. At higher T_{stop} values, the increase in E_a suggests the progressive involvement of deeper and/or overlapping trapping levels, consistent with the hierarchical trapping scenario. The E_a–T_{stop} curve indicates a multi-trap structure that is consistent with a single dominant main peak accompanied by additional shallow and deeper components in the forthcoming deconvolution analysis; however, it should be regarded as providing constraining information on the hierarchy and possible number of peaks rather than determining them directly.

Importantly, the effective activation energy obtained within the plateau region is consistent with the deep-trap values derived independently from the VHR analyses (Hoogenstraaten and BBP methods), supporting a coherent picture of the trap depth associated with the main dosimetric peak and the presence of a stable deep trapping level in $BaZr(BO_3)_2$.

Overall, the observed increase–plateau–increase behaviour of the T_m–T_{stop} curve indicates a hierarchical trapping structure consisting of shallow unstable traps, a dominant thermally isolated trap responsible for the main TL peak, and additional deeper trapping levels contributing at higher temperatures.

For the implementation of the initial rise (IR) method, careful selection of the temperature interval is essential to ensure the validity of the analysis. In the present study, the IR region was defined by selecting a narrow temperature range on the low-temperature side of the main dosimetric peak, where the TL intensity is sufficiently above the background level. The lower bound (T_{min}) was chosen such that the signal exceeds the background noise, while the upper bound (T_{max}) was restricted to temperatures corresponding to less than approximately 5% of the maximum peak intensity (I_{max}).

In practice, this corresponds to a temperature interval of approximately 140–180 °C for the main dosimetric peak. This interval lies entirely within the initial rise region where the TL intensity remains below ~5% of I_{max}, consistent with recommendations that only the low-intensity portion of the glow curve should be used in IR analysis to ensure negligible trap depletion (Coleman and Yukihara, 2018).

4.3. Glow curve deconvolution based on general-order kinetics

GCD based on general-order kinetics was employed to resolve the complex TL glow curve into a set of individual trapping components. In this approach, each glow peak is described by four fundamental parameters: the maximum intensity I_m, the peak temperature T_m, the activation energy E, and the kinetic order b, which collectively govern the trapping and recombination dynamics. The GCD analysis was performed using the tgcd R package (Peng et al., 2016), starting from initial parameter estimates for E and T_m obtained from the VHR and T_m–T_{stop} analyses, with the kinetic order constrained to physically reasonable values close to unity, consistent with general-order TL kinetics. Within the general-order formalism (G mez Ros and Kitis, 2002), the TL intensity as a function of temperature is expressed as:

$$I(T) = I_m \exp\left(\frac{E}{kT_m^2}(T - T_m)\right)\left[\frac{1}{b} + \frac{b-1}{b}\exp\left(\frac{E}{kT_m^2}(T - T_m)\right)\right]^{-\frac{b}{b-1}} \quad (6)$$

This formulation enables an accurate representation of glow peaks exhibiting intermediate kinetic behaviour, where deviations from ideal first- or second-order kinetics arise due to retrapping, competition between traps, or a quasi-continuous distribution of trapping states. Consequently, the general-order model provides a more flexible and physically realistic framework for analyzing non-ideal TL systems with overlapping peaks. In the present case, preliminary fits assuming pure first-order ($b = 1$) kinetics led to noticeably larger figures of merit and structured residuals, especially in the high-temperature wing of the main peak, whereas allowing b to vary slightly above unity significantly improved the fit quality.

Based on the constraints provided by the IR and T_m–T_{stop} diagnostics (single dominant trap in the 125–200 °C plateau region) and the requirement of physically reasonable parameter values, the experimental TL glow curve was deconvoluted using a model with seven peaks. The experimental TL glow curve was successfully deconvoluted into seven individual peaks using the general-order GCD approach implemented in the *tgcd* R package (Peng et al., 2016), as illustrated in Fig. 8. The fitted curve shows excellent agreement with the experimental data, with a figure of merit (FOM) of 2.56%, indicating a reliable reconstruction of the glow curve. Tests with 5–6 peaks resulted in systematically larger FOM values (>4%) and systematic residual trends, whereas increasing the number of peaks beyond seven did not significantly improve the fit quality and led to poorly constrained parameters. The extracted kinetic parameters are summarized in Table 2. The activation energies span a range of ~0.86–1.61 eV, suggesting the presence of multiple trapping levels with varying thermal stabilities. The lower-energy traps (≈0.86–1.07 eV) are associated with relatively shallow trapping centers, while the higher-energy traps (>1.3 eV) correspond to deeper, more stable traps that are likely responsible for the dosimetric TL signal. In particular, the sixth peak ($E \approx 1.44$ eV, $T_m \approx 228$ °C) closely matches the trap depth determined independently from the VHR and IR/T_m–T_{stop} methods for the main dosimetric peak, supporting its assignment as a likely dominant dosimetric component.

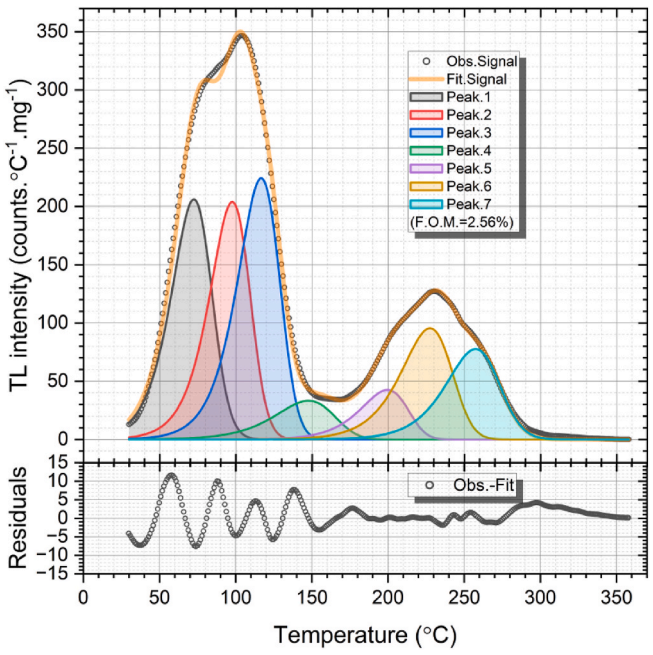

Fig. 8. Glow curve deconvolution of the TL signal of $BaZr(BO_3)_2$ phosphor using the general-order kinetic model. The experimental data (open circles), fitted curve (solid line), and seven individual peaks are shown. Residuals (Obs.–Fit) are presented in the lower panel. The figure of merit (FOM = 2.56%) indicates good agreement between the experimental and fitted curves.

Table 2
Kinetic parameters of the deconvoluted TL glow peaks of $BaZr(BO_3)_2$ phosphor obtained using the general-order kinetic model. The parameters include activation energy (E_a), peak temperature (T_m), initial and final half-width temperatures (T_{m1}, T_{m2}), kinetic order (b), symmetry factor (μ), and frequency factor (s).

Peaks	E_a (eV)	T_m (°C)	T_{m1} (°C)	T_{m2} (°C)	b	μ	s (s^{-1})
1st Peak	0.91	72.80	54.57	86.33	1.31	0.426	3.26×10^{12}
2nd Peak	1.02	97.80	79.58	111.27	1.24	0.425	1.25×10^{13}
3rd Peak	1.07	116.80	97.70	130.80	1.22	0.423	1.11×10^{13}
4th Peak	0.86	147.80	120.66	167.23	1.15	0.417	$2.23 \times 10^{\circ 9}$
5th Peak	1.34	199.80	177.75	214.95	1.12	0.407	2.71×10^{13}
6th Peak	1.44	227.80	204.41	244.31	1.18	0.414	4.19×10^{13}
7th Peak	1.61	256.80	233.66	275.61	1.29	0.448	2.60×10^{14}

The kinetic order values lie in the range $b \approx 1.12$–1.31, indicating that all peaks follow general-order kinetics with slight deviation from first-order behaviour. Such b values only moderately exceed unity and should therefore be interpreted as indicative of moderate retrapping and competition effects, rather than strictly first-order behaviour.

Furthermore, the E–T_{stop} behaviour observed in Fig. 7b shows a progressive increase of the apparent activation energy with increasing T_{stop}, which is characteristic of a distribution of trap depths rather than a single discrete trapping level. In such cases, the activation energies derived from the initial rise method reflect the progressive emptying of the lower-energy side of the distribution as the preheat temperature increases, rather than a unique trap depth.

This interpretation closely parallels the behaviour reported for feldspars and disordered materials, where thermoluminescence signals arise from quasi-continuous distributions of activation energies and frequency factors (Pagonis et al., 2014; McKeever and Sholom, 2021). Within this framework, the TL glow curve can be effectively represented as a superposition of multiple individual components, each corresponding to a limited energy interval within the overall distribution.

Accordingly, the general-order glow-curve deconvolution employed in the present work should be regarded as a semi-empirical approximation of a distributed trapping system, rather than a strict decomposition into discrete, independent trap levels. The activation energies obtained from GCD are therefore interpreted as effective parameters describing different regions of the trap distribution, rather than a single dominant trap.

Independent diagnostics indicate that the dominant dosimetric peak exhibits behaviour close to first-order kinetics, as evidenced by the stability of T_m with increasing dose and the presence of a well-defined plateau in the T_m–T_{stop} plot. It is well established that in interactive multiple trap systems (IMTS), the overall TL behaviour often approaches first-order kinetics, particularly for lower-temperature peaks, as shown by Chen and Pagonis (2013). However, this behaviour reflects the global response of the system, and the effective kinetic order may exhibit a distribution around unity rather than a strict $b = 1$ condition in complex multi-trap systems. Within this framework, the general-order formalism is employed as a semi-empirical tool to describe overlapping components. Constraining the kinetic order strictly to $b = 1$ resulted in poorer fits and structured residuals, whereas allowing small deviations from unity ($b \approx 1.1$–1.3) significantly improved the fit quality. These deviations are therefore interpreted as effective, model-dependent parameters reflecting peak overlap and possible retrapping effects, rather than intrinsically non-first-order kinetics. Accordingly, the deconvolution results should be regarded as a physically consistent, but not unique, representationof the glow curve.

Thus, in agreement with previous discussions on the model-dependence and non-uniqueness of glow-curve deconvolution, the seven-peak general-order solution in $BaZr(BO_3)_2$ is used primarily as a constrained, semi-empirical description of the multi-trap structure, while the underlying first-order-like kinetics of the dominant trap is established independently by VHR, IR and T_m–T_{stop} diagnostics.

This suggests the presence of moderate retrapping and competitive recombination processes, rather than purely first-order kinetics. Furthermore, the distribution of peak temperatures (≈73–257 °C) reflects a broad trap distribution, consistent with a multi-level trapping system. The higher-temperature peaks, particularly those above ~200 °C, are attributed to deeper traps that contribute to the stable dosimetric signal, whereas the lower-temperature peaks are likely associated with less stable trapping centers. It should be emphasized that GCD solutions are generally non-unique and that the seven-peak general-order model represents a self-consistent and physically plausible description, supported by independent VHR, IR, and Tm–Tstop analyses, rather than a unique mapping of individual defects.

Overall, the GCD analysis reveals that the TL response of $BaZr(BO_3)_2$ originates from a complex trap structure with multiple overlapping components, and that the general-order kinetic model provides a consistent semi-empirical description of the recombination dynamics in this material when interpreted together with the complementary kinetic diagnostics.

Although the seven-peak general-order model provides an excellent fit to the experimental glow curve (FOM ≈ 2.6%) and is supported by independent VHR, IR, and T_m–T_{stop} analyses, glow-curve deconvolution remains inherently model-dependent and non-unique. Different combinations of peak numbers and kinetic formalisms may yield comparable fits with varying parameter sets. Therefore, the present GCD solution should be considered a physically consistent, but not uniquely determined, description of the multi-trap system in $BaZr(BO_3)_2$, and the extracted parameters are best interpreted in conjunction with complementary kinetic methods rather than as a direct mapping of specific defect centers. At a heating rate of 2 °C/s, the temperature lag is

estimated to be approximately 5–6 °C (Fig. 5b). This may introduce a systematic shift in the extracted kinetic parameters, particularly for temperature-dependent methods such as IR. However, the consistency between VHR (with correction), IR, and GCD results suggests that this effect does not significantly alter the physical interpretation of the trapping structure, but rather contributes to the overall uncertainty. This is further supported by the consistency between the deep-trap activation energies obtained from VHR (with temperature-lag correction, ~1.7–1.8 eV), IR/T_m–T_{stop} diagnostics, and the GCD results for the main dosimetric component (E ≈ 1.44 eV, T_m ≈ 228 °C), all of which indicate the presence of a dominant deep trapping level within a hierarchical multi-trap system.

In addition, the observed decrease in TL peak area with increasing heating rate (Fig. 5a) indicates the presence of thermal quenching. This effect is known to influence the evaluation of kinetic parameters, particularly the activation energy (E) and kinetic order (b).

In the present study, no independent determination of thermal quenching parameters (e.g., W and C) was performed, and therefore no explicit correction for quenching was applied. As a result, the kinetic parameters obtained from VHR, IR, and GCD analyses should be regarded as effective values that may include an additional systematic uncertainty due to uncorrected thermal quenching.

Nevertheless, these effective parameters define a broadly consistent energy range; however, the activation energies obtained from IR and GCD (~1.4–1.6 eV) are systematically lower than those derived from VHR (~1.7–1.8 eV, after temperature-lag correction). This difference is attributed to the combined influence of thermal quenching, temperature lag, and the distributed nature of the trapping system, which tend to underestimate the apparent activation energy in IR and peak-shape-based methods. Previous analyses (Subedi et al., 2011) have shown that, even in the presence of thermal quenching, key glow curve characteristics such as the peak maximum temperature (T_m), peak intensity, and integrated area can remain comparatively robust, while the activation energy (E) and kinetic order (b) are more strongly affected. Therefore, thermal quenching is expected to introduce a systematic uncertainty in the extracted kinetic parameters rather than altering the overall physical interpretation.

5. Time-dependent fading of TL intensity and integrated signal

The temporal stability of the preheated TL signal was assessed using both the maximum peak intensity (I_m) and the integrated glow-curve area following a preheating protocol of 170 °C for 13 s, selected to strongly suppress the contribution of unstable shallow traps and to isolate the dominant high-temperature dosimetric peak. Fig. 9a shows representative glow curves for different storage durations, while Fig. 9b and c presents the normalized TL peak intensity (I_m) and integrated glow-curve area as functions of fading time, respectively.

Both evaluation methods reveal an overall decay of the TL signal with storage time, accompanied by a pronounced non-monotonic behaviour, particularly in the peak-intensity response. The normalized peak intensity (Fig. 9b) exhibits stronger fluctuations and transient increases at intermediate times, whereas the integrated glow-curve area (Fig. 9c) decreases more gradually and approaches a quasi-plateau at longer storage durations. A pronounced non-monotonic behaviour is observed during the first ~6 h of storage, prior to the onset of the dominant decay regime (Fig. 9b and c). Although this behaviour is unusual for conventional fading, it is not inconsistent with a hierarchical trapping system in which time-dependent charge redistribution can occur after preheating. This behaviour may plausibly be related to the hierarchical trap structure revealed by the T_m–T_{stop} analysis, in which shallow and intermediate traps are progressively emptied while deeper, thermally stable levels are transiently populated via charge redistribution. In this scenario, carriers released from less stable traps are partially retrapped in deeper centers rather than recombining immediately, giving rise to an apparent inverse-fading-like response, analogous to multi-trap competition and redistribution processes reported in borate and feldspar TL systems (Furetta et al., 1999; Chen et al., 2000; Sakurai and Gartia, 1997). It should be noted that the preheating treatment at 170 °C was chosen to strongly reduce the contribution of unstable shallow traps, but it does not necessarily eliminate all intermediate-depth states involved in the hierarchical trap structure. Therefore, charge redistribution from partially depopulated intermediate traps to deeper and more stable levels may still occur during storage. The observed behaviour may also be considered in the broader context of anomalous fading phenomena, which are often attributed to quantum tunneling processes between spatially correlated traps and recombination centers. Although the present data do not allow a definitive identification of such mechanisms, this possibility cannot be excluded and warrants further dedicated investigation.

It is also important to distinguish the fading experiment from the T_m–T_{stop} measurements shown in Fig. 7a. In the T_m–T_{stop} procedure, the TL glow curve is recorded immediately after each preheating step, so the experiment probes instantaneous thermal depletion of traps. In contrast, the fading experiment includes storage times ranging from hours to days after preheating, thereby allowing slower time-dependent processes such as retrapping and charge redistribution to occur. For this reason, the non-monotonic behaviour observed in Fig. 9 is not expected to appear in Fig. 7a. In the context of anomalous fading, it is well known that such behaviour may follow a logarithmic time dependence ($\propto 1/t$), for which a plot of ln (TL) versus ln(t) yields a linear relationship. In the present study, a log–log representation of the TL signal was evaluated (Fig. 9d). The resulting behaviour does not exhibit a simple linear trend over the entire time range, indicating that the fading process does not strictly follow a 1/t dependence. This deviation suggests that the observed behaviour is governed by more complex mechanisms, such as charge redistribution within a hierarchical trap system, rather than a purely tunneling-controlled anomalous fading process.

Such discrepancies between peak-height and area-based evaluations are well known in TL dosimetry, where peak intensity is more sensitive to changes in glow-curve shape, while the integrated area reflects the total number of recombining charge carriers (Benavente et al., 2024; Chen et al., 2015; Pagonis and Chen, 2015). This divergence can be plausibly interpreted in terms of charge redistribution within a multi-trap system. T_m–T_{stop} analysis indicates the presence of shallow, intermediate, and deep trapping levels, with a dominant thermally stable trap governing the main dosimetric peak in the ~125–200 °C region. During storage, charge carriers released from shallow or intermediate traps may either recombine (leading to fading) or become retrapped in deeper levels, resulting in redistribution among traps. Previous studies on borate-based and feldspar TL materials have shown that such shallow–deep coupling can produce complex fading behaviour, including transient signal enhancement at intermediate storage times, consistent with the behaviour observed in the present study (Jain and Ankjærgaard, 2011; Bekker et al., 2025; Fitzgerald et al., 2022; França et al., 2022).

Within the general-order kinetic framework, where the kinetic order parameter is slightly greater than unity, moderate retrapping and competition between traps and recombination centers influence both the release kinetics and recombination probability. Storage-induced redistribution can broaden the effective activation-energy distribution of the dominant peak, leading to glow-curve broadening and subtle shape changes. Since the peak intensity depends on both the amplitude and width of the glow peak, such broadening reduces I_m more strongly than the total emitted signal, whereas the integrated area remains comparatively less affected (Pagonis and Kitis, 2012; Gómez-Ros et al., 2006; Zahedifar et al., 2006).

From a dosimetric perspective, the integrated TL glow-curve area (Fig. 9c) therefore represents a more robust and reliable quantity, as it averages over moderate variations in peak shape and minimizes the influence of peak broadening or slight shifts in T_m (Kitis and Pagonis, 2023; Soliman et al., 2017). While the non-monotonic short-term

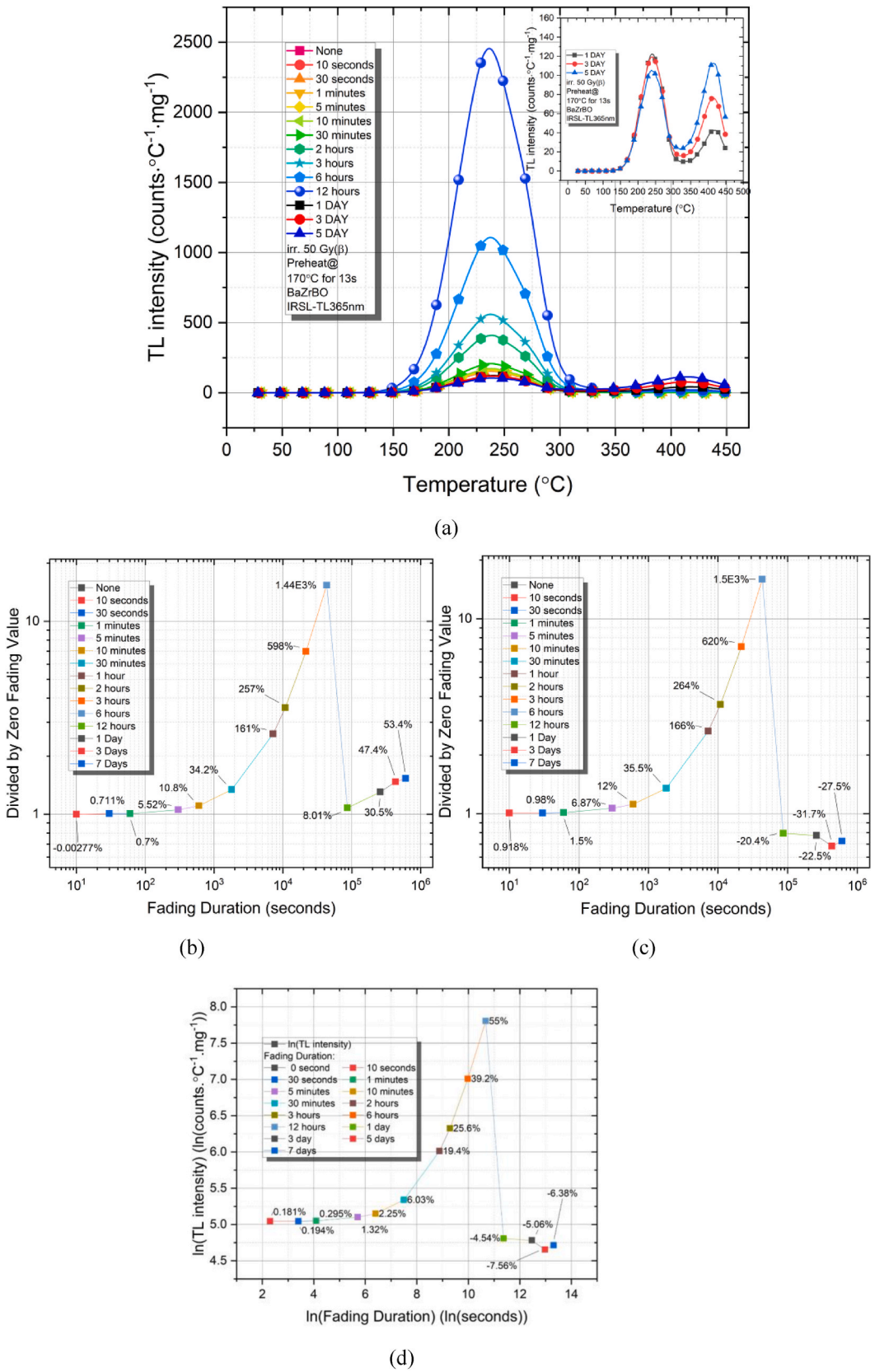

Fig. 9. Fading behaviour of the TL signal of $BaZr(BO_3)_2$ phosphor following a preheating protocol of 170 °C for 13 s: (a) TL glow curves recorded after different storage durations; the inset highlights the evolution of the glow curve at longer storage times; (b) normalized integrated TL glow-curve area as a function of fading duration; (c) normalized TL peak intensity (I_m) as a function of fading duration. (d) Log–log plot of the TL signal (ln (TL)) as a function of fading time (ln(t)). The non-linear behaviour indicates a deviation from the expected $1/t$ dependence.

behaviour requires further dedicated investigation, the longer-term fading of the integrated TL signal remains moderate and is more relevant for practical dosimetric assessment. The residual fading of the integrated signal reflects the finite lifetime of the dominant deep trap and its partial coupling to shallower levels, and is consistent with the behaviour reported for borate-based TL phosphors exhibiting good long-term stability over storage periods of days to weeks.

All TL measurements were performed under identical readout conditions (heating rate, detection window, and preheating protocol), ensuring consistency in the comparison of peak intensity and integrated signal.

6. Conclusions

The present study shows that microwave-assisted sol–gel autocombustion synthesis yields single-phase trigonal $BaZr(BO_3)_2$ with intrinsic TL trapping centers, without requiring extrinsic dopants and underscoring defect-related luminescence in the host lattice. Optimization of the readout conditions (365 nm detection and 170 °C/13 s preheating) effectively suppresses unstable shallow traps and isolates a well-defined dosimetric peak at ~226 °C.

$BaZr(BO_3)_2$ exhibits a linear dose–response up to ~20 Gy, followed by a supralinear regime extending to 500 Gy without observable saturation, a sub-hundred-mGy minimum detectable dose, and cycle-to-cycle reproducibility within ±3–5%, making it competitive among borate-based TL dosimeters for low–intermediate doses. Kinetic analyses consistently indicate a dominant deep trap with activation energies of ~1.7–1.8 eV (after temperature-lag correction) and general-order kinetics slightly above first order, embedded in a hierarchical system of shallow, intermediate and deep levels identified by T_m–T_{stop} and glow-curve deconvolution.

The non-monotonic fading, characterized by an initial signal enhancement followed by gradual decay and a comparatively stable integrated TL signal, is attributed to charge redistribution within this multi-trap system and supports its practical dosimetric applicability. Overall, $BaZr(BO_3)_2$ emerges as a promising intrinsic TL phosphor with stable deep trapping characteristics, while also providing insight into defect-driven TL in undoped borate hosts.

CRediT authorship contribution statement

M. Oglakci: Formal analysis, Investigation, Methodology. **Abeer S. Altowyan:** Formal analysis, Funding acquisition, Investigation, Methodology, Writing – original draft. **T. Karaman:** Formal analysis, Investigation, Methodology. **E.A. Cin:** Formal analysis, Investigation, Methodology. **O.T. Ozmen:** Conceptualization, Investigation. **Jabir Hakami:** Conceptualization, Investigation. **O. Madkhali:** Conceptualization, Methodology. **M.B. Coban:** Formal analysis, Investigation, Methodology. **U.H. Kaynar:** Investigation, Methodology. **N. Can:** Supervision, Writing – original draft, Writing – review & editing.

Declaration of Competing Interest

The authors declare that they have no known competing financial interests or personal relationships that could have appeared to influence the work reported in this paper.

Acknowledgements

The authors gratefully acknowledge the funding of the Princess Nourah bint Abdulrahman University Researchers Supporting Project (Project No. PNURSP2026R16), Princess Nourah bint Abdulrahman University, Riyadh, Saudi Arabia.

Data availability

Data will be made available on request.

References

Alajlani, Y., Oglakci, M., Kaynar, U.H., Ayvacikli, M., Portakal-Uçar, Z.G., Topaksu, M., Can, N., 2021. Thermoluminescence study and evaluation of trapping parameters of samarium doped barium silicate phosphor. J. Asian Ceram. Soc. 9, 291–303. https://doi.org/10.1080/21870764.2020.1864898.

Alathlawi, H.J., Barad, A., Madkhali, O., Souadi, G., Sharahili, M., Hakami, J., Balci, S., Kaynar, U.H., Topaksu, M., Can, N., 2025. Intrinsic thermoluminescence and anomalous heating rate effects in undoped $K_7SrY_2(B_5O_{10})_3$ phosphors: a combined Tm–Tstop and GOK deconvolution study. Appl. Radiat. Isot. 225, 112092. https://doi.org/10.1016/j.apradiso.2025.112092.

Alshoaibi, A., Ike, P.O., Nwanya, A.C., Awada, C., Islam, S., Ezema, F.I., 2023. Effect of Mg on the structural, optical and thermoluminescence properties of $Li_3Al_3(BO_3)_4$: shift in main glow peak. Molecules 28, 504. https://doi.org/10.3390/molecules28020504.

Altowyan, A.S., Sonsuz, M., Kaynar, U.H., Hakami, J., Portakal-Uçar, Z.G., Ayvacikli, M., Topaksu, M., Can, N., 2024. Synthesis and thermoluminescence behavior of novel Sm^{3+} doped $YCa_4O(BO_3)_3$ under beta irradiation. Ceram. Int. 50, 19681–19691. https://doi.org/10.1016/j.ceramint.2024.03.089.

Anishia, S.R., Jose, M.T., Annalakshmi, O., Ramasamy, V., 2011. Thermoluminescence properties of rare Earth doped lithium magnesium borate phosphors. J. Lumin. 131, 2492–2498. https://doi.org/10.1016/j.jlumin.2011.06.019.

Bakr, M., Portakal-Uçar, Z.G., Yüksel, M., Kaynar, Ü.H., Ayvacikli, M., Benourdja, S., Canimoglu, A., Topaksu, M., Hammoudeh, A., Can, N., 2020. Thermoluminescence properties of beta particle irradiated $Ca_3Al_2O_6$ phosphor relative to environmental dosimetry. J. Lumin. 227, 117565. https://doi.org/10.1016/j.jlumin.2020.117565.

Balci-Yegen, S., Boronat, C., Garcia-Guinea, J., Topaksu, M., Correcher, V., 2018. Correlation between thermoluminescence emission and phase transitions of tridymite. Phase Transitions 91, 1122–1128. https://doi.org/10.1080/01411594.2018.1515435.

Bekker, T.B., Davydov, A.V., Ryadun, A.A., Yelisseyev, A.P., Solntsev, V.P., Fedorenko, A. D., 2025. Examining the contribution of Cu and Sr codoping on luminescence properties of borate crystals. Opt. Mater. 158, 116465. https://doi.org/10.1016/j.optmat.2024.116465.

Benavente, J.F., Arquero, O., Berenguer-Antequera, J., 2024. Effects of trapped charge transitions between localized levels on the optical properties of thermoluminescent materials: a study of fading and thermal quenching. Opt. Mater. 156, 116006. https://doi.org/10.1016/j.optmat.2024.116006.

Benavente, J.F., Gómez-Ros, J.M., Correcher, V., 2020. Characterization of the thermoluminescence glow curve of $Li_2B_4O_7$:Cu,Ag. Radiat. Meas. 137, 106427. https://doi.org/10.1016/j.radmeas.2020.106427.

Bohun, A., 1954. Thermoemission und Photoemission von Natriumchlorid, Czechoslov. J. Phys. (Paris) 4, 91–93. https://doi.org/10.1007/BF01688114.

Booth, A.H., 1954. Calculation of electron trap depths from thermoluminescence maxima. Can. J. Chem. 32, 214–215. https://doi.org/10.1139/v54-027.

Bos, A., 2017. Thermoluminescence as a research tool to investigate luminescence mechanisms. Materials 10, 1357. https://doi.org/10.3390/ma10121357.

Castro, S., Gayoso, M., Rivas, J., Greneche, J.M., Mira, J., Rodríguez, C., 1996. Structural and magnetic properties of barium hexaferrite nanostructured particles prepared by the combustion method. J. Magn. Magn Mater. 152, 61–69. https://doi.org/10.1016/0304-8853(95)00450-5.

Chandrasekhar, M., 2025. Thermoluminiscene parameters of neodymium doped Y_2O_3 nanophosphors. J. Appl. Sci. Eng. Technol. 1. https://doi.org/10.64164/JASET250101004.

Chen, R., 1969. Glow curves with general order kinetics. J. Electrochem. Soc. 116, 1254. https://doi.org/10.1149/1.2412291.

Chen, R., Leung, P.L., Stokes, M.J., 2000. Apparent anomalous fading of thermoluminescence associated with competition with radiationless transitions. Radiat. Meas. 32, 505–511. https://doi.org/10.1016/S1350-4487(00)00082-2.

Chen, R., Pagonis, V., Lawless, J.L., 2015. Time and dose-rate dependence of TL and OSL due to competition between excitation and fading. Radiat. Meas. 82, 115–121. https://doi.org/10.1016/j.radmeas.2015.09.006.

Chen, Z., Yan, Y., Liu, J., Yin, Y., Wen, H., Zao, J., Liu, D., Tian, H., Zhang, C., Li, S., 2009. Microwave induced solution combustion synthesis of nano-sized phosphors. J. Alloys Compd. 473, L13–L16. https://doi.org/10.1016/j.jallcom.2008.05.060.

Chen, R., McKeever, S.W.S., 1997. Theory of Thermoluminescence and Related Phenomena. World Scientific. https://doi.org/10.1142/2781.

Chen, R., Pagonis, V., 2013. On the expected order of kinetics in a series of thermoluminescence (TL) and thermally stimulated conductivity (TSC) peaks. Nucl. Instrum. Methods Phys. Res. Sect. B Beam Interact. Mater. Atoms 312, 60–69. https://doi.org/10.1016/j.nimb.2013.07.008.

Chen, V., R, 2011. Pagonis, Thermoluminescence of Solids. Springer.

Cin, E.A., Bulcar, K., Altowyan, A.S., Coban, M.B., Kaynar, U.H., Ozmen, O.T., Hakami, J., Aydin, H., Canimoglu, A., Topaksu, M., Can, N., 2026. Non-classical thermoluminescence kinetics and inverse fading behavior in $K_7CaGd_2(B_5O_{10})_3$ phosphor. Radiat. Phys. Chem. 244, 113778. https://doi.org/10.1016/j.radphyschem.2026.113778.

Coleman, A.C., Yukihara, E.G., 2018. On the validity and accuracy of the initial rise method investigated using realistically simulated thermoluminescence curves. Radiat. Meas. 117, 70–79. https://doi.org/10.1016/j.radmeas.2018.07.010.

Daniel, D.J., Kim, H.J., Kim, S., Kothan, S., Kaewkhao, J., 2019. Trap level analysis of Ce^{3+} and Sm^{3+} in $Li_6Y(BO_3)_3$. Ceram. Int. 45, 11893–11898. https://doi.org/10.1016/j.ceramint.2019.03.072.

Del Sol Fernández, S., García-Salcedo, R., Mendoza, J.G., Sánchez-Guzmán, D., Rodríguez, G.R., Gaona, E., Montalvo, T.R., 2016. Thermoluminescent characteristics of LiF:Mg, Cu, P and $CaSO_4$:Dy for low dose measurement. Appl. Radiat. Isot. 111, 50–55. https://doi.org/10.1016/j.apradiso.2016.02.011.

Deng, Y., Gao, Y., Zhu, F., Zhu, B., Huang, L., Qiu, J., 2024. Sol-gel combustion synthesis and near-infrared luminescence of Ni^{2+}-doped $MgAl_2O_4$ spinel phosphor. Ceram. Int. 50, 12319–12325. https://doi.org/10.1016/j.ceramint.2024.01.136.

Ding, Z., Huang, X., Liu, W., Kim, I.J., Han, Y.-H., 2021. Preparation of high-temperature active zirconium boride powders via precursor route and microwave sintering. Adv. Appl. Ceram. 120, 222–226. https://doi.org/10.1080/17436753.2021.1933839.

Dogan, T., Tormo, L., Akca, S., Kucuk, N., Guinea, J.G., Karabulut, Y., Ayvacikli, M., Oglakci, M., Topaksu, M., Can, N., 2019. Cathodoluminescence and thermoluminescence of ZnB_2O_4:Eu^{3+} phosphors prepared via wet-chemical synthesis. Ceram. Int. 45, 4918–4925. https://doi.org/10.1016/j.ceramint.2018.11.191.

Encinas-Osuna, I.G., Bernal, R., Cortez-Galaz, C., Cruz-Vázquez, C., 2023. Persistent luminescence dosimetry performance of solid state synthesized $BaZrO_3$ phosphors. Appl. Radiat. Isot. 199, 110909. https://doi.org/10.1016/j.apradiso.2023.110909.

Fitzgerald, S.K., Sanderson, D.C.W., Cresswell, A.J., Martin, L., 2022. Using Infra-red stimulated luminescence and phototransferred thermoluminescence to investigate electron trapping and charge transport in feldspars. Radiat. Meas. 156, 106817. https://doi.org/10.1016/j.radmeas.2022.106817.

França, L.V.S., Borges, F.H., Gonçalves, R.R., Baffa, O., Yukihara, E.G., 2022. Influence of lanthanide (gd, Tb or ce) and silver doping on the luminescence lifetimes of calcium borate investigated by pulsed optically stimulated luminescence. J. Lumin. 248, 118809. https://doi.org/10.1016/j.jlumin.2022.118809.

Furetta, C., Kitis, G., Weng, P.S., Chu, T.C., 1999. Thermoluminescence characteristics of MgB_4O_7: dy,na. Nucl. Instruments Methods Phys. Res. Sect. A Accel. Spectrometers, Detect. Assoc. Equip. 420, 441–445. https://doi.org/10.1016/S0168-9002(98)01198-X.

G mez Ros, J.M., Kitis, G., 2002. Computerised glow curve deconvolution using general and mixed order kinetics. Radiat. Protect. Dosim. 101, 47–52. https://doi.org/10.1093/oxfordjournals.rpd.a006029.

Gardenali Yukihara, E., 2023. TL and OSL as research tools in luminescence: possibilities and limitations. Ceram. Int. 49, 24356–24369. https://doi.org/10.1016/j.ceramint.2022.10.199.

Gartia, R.K., Ingotombi, S., Sing, T.S.S., Mazumdar, P.S., 1991. On the determination of the activation energy of a thermoluminescence peak by the two-heating-rates method. J. Phys. D Appl. Phys. 24, 65–69. https://doi.org/10.1088/0022-3727/24/1/011.

Gavhane, K.H., Bhadane, M.S., Bhoir, A.S., Kulkarni, P.P., Patil, B.J., Bhoraskar, V.N., Dhole, S.D., Dahiwale, S.S., 2020. Tm-Tstop analysis and dosimetric properties of Ce doped BaB_4O_7 phosphor. J. Alloys Compd. 817, 152805. https://doi.org/10.1016/j.jallcom.2019.152805.

Gómez-Ros, J.M., Furetta, C., Correcher, V., 2006. Simple methods to analyse thermoluminescence glow curves assuming arbitrary recombination–retrapping rates. Radiat. Protect. Dosim. 119, 339–343. https://doi.org/10.1093/rpd/nci523.

Guo, H., Wang, Y., Li, G., Liu, J., Feng, P., Liu, D., 2017. Cyan emissive super-persistent luminescence and thermoluminescence in $BaZrSi_3O_9$:Eu^{2+},Pr^{3+} phosphors. J. Mater. Chem. C 5, 2844–2851. https://doi.org/10.1039/C7TC00133A.

Halefoglu, Y.Z., Oglakci, M., Portakal, Z.G., Akca, S., Souadi, G.O., Canimoglu, A., Topaksu, M., Can, N., 2020. A study on thermoluminescence behaviour of Eu doped LaB_3O_6 irradiated with beta particles. Radiat. Phys. Chem. 168, 108571. https://doi.org/10.1016/j.radphyschem.2019.108571.

Hoogenstraaten, W., 1958. Electron Traps in zinc-sulphide Phosphors. Faculteit der Wis-en Natuurkunde Universiteit van Amsterdam.

Hornebecq, V., Gravereau, P., Chaminade, J.P., Lebraud, E., 2002. $BaZr(BO_3)_2$: a non-centrosymmetric dolomite-type superstructure. Mater. Res. Bull. 37, 2165–2178. https://doi.org/10.1016/S0025-5408(02)00899-1.

Jain, M., Ankjærgaard, C., 2011. Towards a non-fading signal in feldspar: insight into charge transport and tunnelling from time-resolved optically stimulated luminescence. Radiat. Meas. 46, 292–309. https://doi.org/10.1016/j.radmeas.2010.12.004.

Joseph, T.A., Chopra, V., Dhoble, S.J., 2023. Thermoluminescence studies of zinc borate (ZnB_2O_4) phosphor doped with rare earths for dosimetric aspects. Luminescence 38, 1597–1606. https://doi.org/10.1002/bio.4542.

Ju, G., Hu, Y., Chen, L., Jin, Y., Li, Y., 2017. Persistent luminescence in the self-activated $K_2Zr(BO_3)_2$. RSC Adv. 7, 4190–4195. https://doi.org/10.1039/C6RA26120E.

Junliang, L., Yanwei, Z., Cuijing, G., Wei, Z., Xiaowei, Y., 2010. One-step synthesis of barium hexaferrite nano-powders via microwave-assisted sol–gel auto-combustion. J. Eur. Ceram. Soc. 30, 993–997. https://doi.org/10.1016/j.jeurceramsoc.2009.10.019.

Kalita, J.M., Chithambo, M.L., 2017. The influence of dose on the kinetic parameters and dosimetric features of the main thermoluminescence glow peak in α-Al_2O_3:C,Mg. Nucl. Instrum. Methods Phys. Res. Sect. B Beam Interact. Mater. Atoms 394, 12–19. https://doi.org/10.1016/j.nimb.2016.12.027.

Katyayan, S., Agrawal, S., 2019. Optical behavior and TL kinetics of Eu^{3+} and Tb^{3+} doped zirconate thermoluminescent phosphors. Opt. Quant. Electron. 51, 277. https://doi.org/10.1007/s11082-019-1993-7.

Kaynar, Ü.H., Oglakci, M., Bulcar, K., Benourdja, S., Bakr, M., Ayvacikli, M., Canimoglu, A., Topaksu, M., Can, N., 2023. Comparison of thermoluminescence characteristics of undoped and europium doped $YAl_3(BO_3)_4$ phosphor synthesized by combustion method: anomalous heating rate, dose response and kinetic analyses. Radiat. Phys. Chem. 204, 110657. https://doi.org/10.1016/j.radphyschem.2022.110657.

Kitis, G., Pagonis, V., 2017. New expressions for half life, peak maximum temperature, activation energy and kinetic order of a thermoluminescence glow peak based on the lambert W function. Radiat. Meas. 97, 28–34. https://doi.org/10.1016/j.radmeas.2016.12.013.

Kitis, G., Pagonis, V., 2023. Simulation of thermoluminescence signals at very low dose rates and low doses: implications for dosimetric applications. Radiat. Phys. Chem. 209, 110968. https://doi.org/10.1016/j.radphyschem.2023.110968.

Kitis, G., Tuyn, J.W.N., 1998. A simple method to correct for the temperature lag in TL glow-curve measurements. J. Phys. D Appl. Phys. 31, 2065–2073. https://doi.org/10.1088/0022-3727/31/16/017.

Kucuk, N., 2019. Thermoluminescence characteristics of terbium doped zinc borates. Crystals 9, 557. https://doi.org/10.3390/cryst9110557.

Kumar, B.A., Bindu, P.H., 2022. Advances in borate- and phosphate-based TL materials for in vivo dosimetry. J. Korean Ceram. Soc. 59, 537–550. https://doi.org/10.1007/s43207-022-00240-x.

Leon, M., Montes, E., Elias, J.A., Cervantes, J.L., Diaz-Torres, L.A., Sosa, M.A., Vallejo, M. A., 2024. Effect of the crystalline phase type on the thermoluminescent response of ZrO_2 due to different synthesis methods. Nano 19. https://doi.org/10.1142/S1793292024500395.

Liu, L., Wang, L., Pang, R., Jiang, L., Zhang, Y., Chen, X., Han, Z., Yu, Z., 2025. Study of thermoluminescence and trapping parameter evaluation of $Ba_2Mg(BO_3)_2$:RE^{3+} (RE = Dy, Tb and tm) exposed to beta ray irradiation. Radiat. Eff. Defect Solid 180, 1259–1269. https://doi.org/10.1080/10420150.2025.2458329.

Liuzzi, R., Piccolo, C., D'Avino, V., Clemente, S., Oliviero, C., Cella, L., Pugliese, M., 2020. Dose–response of TLD-100 in the dose range useful for hypofractionated radiotherapy. Dose Response 18. https://doi.org/10.1177/1559325819894081.

Madkhali, O., Bulcar, K., Barad, A., Zelai, T., Souadi, G., Alathlawi, H.J., Kaynar, U.H., Topaksu, M., Can, N., 2025. Thermoluminescence behaviour and kinetic analysis of a novel Tb^{3+}-Doped $LaCa_4O(BO_3)_3$ phosphor: impacts of heating rates and dose. Mater. Sci. Semicond. Process. 187, 109132. https://doi.org/10.1016/j.mssp.2024.109132.

Manju, P., Ajith, M.R., Jaiswal-Nagar, D., 2019. Synthesis and characterization of $BaZrO_3$ nanoparticles by citrate-nitrate sol-gel auto-combustion technique: systematic study for the formation of dense $BaZrO_3$ ceramics. J. Eur. Ceram. Soc. 39, 3756–3767. https://doi.org/10.1016/j.jeurceramsoc.2019.03.048.

McKeever, S.W.S., 1980. On the analysis of complex thermoluminescence. Glow-curves: resolution into individual peaks. Phys. Status Solidi A Appl. Mater. Sci. 62, 331–340. https://doi.org/10.1002/pssa.2210620139.

McKeever, S.W.S., 1985. Thermoluminescence of Solids. Cambridge University Press. https://doi.org/10.1017/CBO9780511564994.

McKeever, S.W.S., 2025. Glow curve deconvolution – why are Most published results wrong? Common pitfalls in measurement and analysis. Radiat. Meas. 189, 107537. https://doi.org/10.1016/j.radmeas.2025.107537.

McKeever, S.W.S., Sholom, S., 2021. Trap level spectroscopy of disordered materials using thermoluminescence: an application to aluminosilicate glass. J. Lumin. 234, 117950. https://doi.org/10.1016/j.jlumin.2021.117950.

Mączka, M., Szymborska-Małek, K., Gągor, A., Majchrowski, A., 2015. Growth and characterization of acentric $BaHf(BO_3)_2$ and $BaZr(BO_3)_2$. J. Solid State Chem. 225, 330–334. https://doi.org/10.1016/j.jssc.2015.01.008.

Menezes, D. de L.A., Zanatta, K.C., Bannwart, E.S., Antonelli, E., Rodriguez Chialanza, M., Azcune, G., De Souza, J.E., Rojas de Souza, S., 2024. Structural and thermoluminescence properties of lithium borate glass matrices under UV and beta radiation. Luminescence 39. https://doi.org/10.1002/bio.4732.

Nabadwip Singh, S., 2021. Analysis of the thermoluminescent of borate glass by computerized glow curve deconvolution in kinetic formalism. J. Phys., Conf. Ser. 2070, 012009. https://doi.org/10.1088/1742-6596/2070/1/012009.

Nolasco-Altamirano, D., Alonso-Sotolongo, A., Benavente-Cuevas, J.F., García-Salcedo, R., García-Gardunño, O.A., Zarate-Medina, J., Correcher, V., Rivera-Montalvo, T., 2025. Kinetic parameters analysis of $GdAlO_3$ based on thermoluminescent phenomenon. Phys. Status Solidi A Appl. Mater. Sci. 262. https://doi.org/10.1002/pssb.202400381.

Oglakci, M., Akça-Özalp, S., Portakal-Uçar, Z.G., Correcher, V., Benavente, J.F., Sonsuz, M., Can, N., Halefoglu, Y.Z., Topaksu, M., 2025. Thermoluminescence study of Nd^{3+} doped lanthanum tri-borate phosphor. J. Alloys Compd. 1013, 178570. https://doi.org/10.1016/j.jallcom.2025.178570.

Oguntona, K.B., Ogundare, F.O., 2019. Thermoluminescence kinetic parameters of liF: Mg,P. Optik 181, 862–868. https://doi.org/10.1016/j.ijleo.2018.12.155.

Pagonis, V., Kitis, G., Furetta, C., 2006. Numerical and Practical Exercises in Thermoluminescence. Springer New York, New York, NY. https://doi.org/10.1007/0-387-30090-2.

Pagonis, V., Morthekai, P., Kitis, G., 2014. Kinetic analysis of thermoluminescence glow curves in feldspar: evidence for a continuous distribution of energies. Geochronometria 41, 168–177. https://doi.org/10.2478/s13386-013-0148-z.

Pagonis, V., Chen, R., 2015. Monte carlo simulations of TL and OSL in nanodosimetric materials and feldspars. Radiat. Meas. 81, 262–269. https://doi.org/10.1016/j.radmeas.2014.12.009.

Pagonis, V., Kitis, G., 2012. Prevalence of first-order kinetics in thermoluminescence materials: an explanation based on multiple competition processes. Phys. Status Solidi A Appl. Mater. Sci. 249, 1590–1601. https://doi.org/10.1002/pssb.201248082.

Parfianovitch, I.A., 1954. The determination of the depth of electron traps in crystal phosphors. J. Exp. Theor. Phys. 26, 696.

Peng, J., Dong, Z., Han, F., 2016. Tgcd: an R package for analyzing thermoluminescence glow curves. SoftwareX 5, 112–120. https://doi.org/10.1016/j.softx.2016.06.001.

Reddy, S.S., Nagabhushana, K.R., Tatumi, S.H., Thejavathi, N.R., 2025. Investigating the optical and thermoluminescence properties of γ-irradiated $Al_2O_3:Tb^{3+}$ phosphors for dosimetric applications. J. Lumin. 280, 121067. https://doi.org/10.1016/j.jlumin.2025.121067.

Roy, D.J., Choudhari, Y.D., Rewatkar, K.G., Kokode, N.S., Borikar, D.M., 2021. Investigation of structural and dielectric properties of Co-Zr doped Barium M-type Hexaferrites. J. Phys., Conf. Ser. 1913, 012056. https://doi.org/10.1088/1742-6596/1913/1/012056.

Sadek, A.M., Eissa, H.M., Basha, A.M., Kitis, G., 2015. Properties of the thermoluminescence glow peaks simulated by the interactive multiple-trap system (IMTS) model. Phys. Status Solidi A Appl. Mater. Sci. 252, 721–729. https://doi.org/10.1002/pssb.201451406.

Sakurai, T., Gartia, R.K., 1997. Evidence of continuous trap distribution in the glow curve of a Brown microcline. J. Appl. Phys. 82, 5722–5727. https://doi.org/10.1063/1.366436.

Salas-Juárez, C., Burruel-Ibarra, S.E., Gil-Tolano, M.I., Rodriguez, A.P., Romo-Garcia, F., Garcia-Haro, A.R., Brown, F., Yacaman-Valdez, M., Iriqui-Razcón, J.L., Martínez-Gil, M., Melendrez, R., 2023. Persistent luminescence of $ZrO_2:Tb^{3+}$ after beta particle irradiation for dosimetry applications. J. Lumin. 257, 119712. https://doi.org/10.1016/j.jlumin.2023.119712.

Satkar, R.C., Kadam, A.R., Ovhal, D.A., Dhoble, S.J., 2021. Inorganic thermoluminescent phosphors in radiation dosimetry: an overview. J. Phys., Conf. Ser. 1913, 012023. https://doi.org/10.1088/1742-6596/1913/1/012023.

Soliman, H.A., Hassan, M.A., Esmat, E., Sadek, A.M., Maghraby, A.M., 2017. Thermally enhanced TLD output: impacts on the response curve. Appl. Radiat. Isot. 125, 60–65. https://doi.org/10.1016/j.apradiso.2017.04.007.

Sonsuz, M., Topaksu, M., Hakami, J., Can, N., 2022. Synthesis and thermoluminescence study of Eu doped novel $LaBO_3$ phosphor: heating rate, dose response, trapping parameters. Radiat. Phys. Chem. 201, 110412. https://doi.org/10.1016/j.radphyschem.2022.110412.

Subedi, B., Oniya, E., Polymeris, G.S., Afouxenidis, D., Tsirliganis, N.C., Kitis, G., 2011. Thermal quenching of thermoluminescence in quartz samples of various origin. Nucl. Instrum. Methods Phys. Res. Sect. B Beam Interact. Mater. Atoms 269, 572–581. https://doi.org/10.1016/j.nimb.2011.01.011.

Sunta, C.M., Kulkarni, R.N., Piters, T.M., Ayta, W.E.F., Watanabe, S., 1998. General order kinetics of thermoluminescence-a comparison with physical models. J. Phys. D Appl. Phys. 31, 2074–2081. https://doi.org/10.1088/0022-3727/31/16/018.

Szumera, M., Łagowska, B., Sułowska, J., Jeleń, P., Olejniczak, Z., Lach, R., Berezicka, A., Kijo-Kleczkowska, A., 2022. Investigating the crystallization process of boron-bearing silicate-phosphate glasses by thermal and spectroscopic methods. Molecules 27, 867. https://doi.org/10.3390/molecules27030867.

Townsend, P.D., Wang, Y., McKeever, S.W.S., 2021. Spectral evidence for defect clustering: relevance to radiation dosimetry materials. Radiat. Meas. 147, 106634. https://doi.org/10.1016/j.radmeas.2021.106634.

Tsoutsoumanos, E., Konstantinidis, P.G., Polymeris, G.S., Karakasidis, T., Kitis, G., 2022. Electron trap filling and emptying through simulations: studying the shift of the maximum intensity position in Thermoluminescence and Linearly Modulated Optically Stimulated luminescence curves. Radiat. Meas. 153, 106735. https://doi.org/10.1016/j.radmeas.2022.106735.

Ullah, B., Kakakhel, M.B., Ur Rehman, S., Siddique, M.T., Munir, M., Ahmad, K., Mahmood, M.M., Wazir-ud-Din, M., Anjum, I., 2024. Synthesis and dosimetric characterization of lithium tetraborate ($Li_2B_4O_7$:Cu,Ag) thermoluminescent dosimeter with improved reproducibility and reusability. Radiat. Phys. Chem. 220, 111704. https://doi.org/10.1016/j.radphyschem.2024.111704.

Wazir-ud-Din, M., Shakeel-ur-Rehman, Poelman, D., De Grave, J., Vandenberghe, D., Basim Kakakhel, M., Hayat, S., Karimi Moayed, N., 2023. Thermoluminescence dosimetric and kinetic characterization of Pakistani fluorite after β irradiation. Nucl. Instrum. Methods Phys. Res. Sect. B Beam Interact. Mater. Atoms 540, 246–258. https://doi.org/10.1016/j.nimb.2023.04.031.

Xiong, P., Zheng, C., Peng, M., Zhou, Z., Xu, F., Qin, K., Hong, Y., Ma, Z., 2020. Self-activated persistent luminescence from $Ba_2Zr_2Si_3O_{12}$ for information storage. J. Am. Ceram. Soc. 103, 6922–6931. https://doi.org/10.1111/jace.17412.

Yamazaki, T., Tomimasu, T., Mikado, T., Chiwaki, M., 1978. On the supralinearity of Mg_2SiO_4 :tb thermoluminescent dosimeters. J. Appl. Phys. 49, 4929–4932. https://doi.org/10.1063/1.325528.

Zahedifar, M., Karimi, L., Kavianinia, M.J., 2006. Thermoluminescence general-order glow curve deconvolution function with continuous distribution of activation energies. Nucl. Instruments Methods Phys. Res. Sect. A Accel. Spectrometers, Detect. Assoc. Equip. 564, 515–520. https://doi.org/10.1016/j.nima.2006.03.016.